UNIVERSITY OF CALIFORNIA,
IRVINE

Edge-averaged virtual element methods for convection-diffusion problems

DISSERTATION

submitted in partial satisfaction of the requirements
for the degree of

DOCTOR OF PHILOSOPHY

in Mathematics

by

Seulip Lee

Dissertation Committee:
Professor Long Chen, Chair
Professor Qing Nie
Professor Jack Xin

2021

TABLE OF CONTENTS

LIST OF FIGURES

LIST OF TABLES

Page

ACKNOWLEDGMENTS

To begin with, I sincerely appreciate my Ph.D. advisor Professor Long Chen who provided advice and lessons in my research field. The guidance of Professor Chen motivated me to become conscious of numerical approaches for convection-diffusion problems in convection-dominated regime. With his wide knowledge, I was able to overcome the difficulties in the development of edge-averaged virtual element methods. Furthermore, I learned about so many valuable lessens in my academic life from Professor Chen, and they will help me make good decisions about my career path.

I was fortunate to meet my collaborator Dr. Shuhao who helped me to involve our research project deeply. Thanks to his concerns and careful advice, I was able to cultivate my mathematical insights for my research area as well as broaden my perspective on my academic career.

I would like to thank Professor Qing Nie and Professor Jack Xin for serving as my committee members and share their insights and expertise on my research. Thanks to my teaching advisor Roberto Pelayo, I was able to enhance my teaching skills and lead students to concentrate on my class. I would also like to thank all Long's group members and my friends at the department of Mathematics in University of California, Irvine for all the time we have spent together.

I was wholeheartedly pleased to have spent my precious time with Floyd Maseda and HaeRee Lee. They were willing not only to support and encourage me whenever I found myself in trouble, but also to present various ideas for living in a foreign country.

Finally, I always feel indebted to my parents for their unstinting support for me and to my fiancé SeongHee Jeong who has stayed by my side and has been my rock anywhere at any time.

VITA

Seulip Lee

EDUCATION

Doctor of Philosophy in Mathematics — **2015 - Current**
University of California, Irvine — *Irvine, California*

Master in Computational Science and Engineering — **2013 - 2015**
Yonsei University — *Seoul, Republic of Korea*

Bachelor of Science in Mathematics — **2006 - 2013**
Yonsei University — *Seoul, Republic of Korea*

RESEARCH EXPERIENCE

Graduate Research Assistant — **2007 - 2012**
University of California, Irvine — *Irvine, California*

TEACHING EXPERIENCE

Teaching Associate — **2021 - Current**
University of California, Irvine — *Irvine, California*

Teaching Assistant — **2017 - Current**
University of California, Irvine — *Irvine, California*

REFEREED JOURNAL PUBLICATIONS

C^0 Interior Penalty Methods for a Dynamic Nonlinear Beam Model **2018**
Applied Mathematics and Computation

ABSTRACT OF THE DISSERTATION

Edge-averaged virtual element methods for convection-diffusion problems

By

Seulip Lee

Doctor of Philosophy in Mathematics

University of California, Irvine, 2021

Professor Long Chen, Chair

We present stabilized virtual element methods for convection-diffusion problems in the convection-dominated regime. In the context of finite element methods, the edge-averaged finite element schemes were successfully applied to convection-dominated problems. We aim to generalize the edge-averaged stabilization to the virtual element framework. Hence, we develop the edge-averaged virtual element methods that produce numerical solutions on polygonal meshes without spurious oscillations caused by small diffusion coefficients. Well-posedness of the discrete problem and convergence analysis are provided. We also show numerical experiments which support theoretical results, and display numerical solutions with sharp boundary layers in the convection-dominated regime.

Chapter 1

Introduction

1.1 Convection-Diffusion Problems

We consider the convection-diffusion equation,

$$-\nabla \cdot (\alpha(\mathbf{x})\nabla u + \boldsymbol{\beta}(\mathbf{x})u) = f \quad \text{in } \Omega$$

where $\Omega \subset \mathbb{R}^2$, $\alpha \in C^0(\bar{\Omega})$ with $0 < \alpha_{\min} \leq \alpha(\mathbf{x}) \leq \alpha_{\max}$ for every $\mathbf{x} \in \Omega$, and $\boldsymbol{\beta} \in (C^0(\bar{\Omega}))^2$. The convection-diffusion problems have been considered in numerous mathematical models of flows and other physical phenomena. The problems express the convective and molecular transport along a stream moving at given velocity $\boldsymbol{\beta}$ and with diffusive effects from α. Generally, *convection-dominated regime* means the situation that

$$\alpha_{\max} \ll |\boldsymbol{\beta}(\mathbf{x})|, \quad \forall \mathbf{x} \in \Omega.$$

The convection-dominated regime plays an important role for solving Navier-Stokes equations with high Raynolds number. It has been shown in [36, 47] that the standard finite

element method (FEM) cannot provide a good approximation for the convection-dominated problems. This phenomenon was verified by mathematical analysis: The upper bound of the error may blow up when α is small (Céa's lemma). The numerical simulation showed that the finite element solutions contain spurious oscillations around sharp boundary layers. Such a numerical solution containing the oscillations is called a non-stable solution, and some advanced schemes to get a solution without the oscillations or with smaller oscillations are considered as stabilized methods.

Many stabilized methods have been developed in the context of FEMs, and they can be classified several categories. The first direction is the development of stabilized methods with a provable order of convergence in appropriate norms by adding more terms to their bilinear forms.

- The *streamline-upwind Petrov-Galerkin* (SUPG) method [27] provides the reasonable coercivity result with a mesh dependent norm.
- The *continuous interior penalty* (CIP) method [28] applies penalty to local outflow boundary of each element.
- The *local projection stabilization* (LPS) method [41] is to add a stabilization term simpler than SUPG method.

Our research focus is on linear stabilized methods that compute numerical solutions without spurious oscillations and still with sharp layers. It is well-known that the numerical solutions u_h without spurious oscillations are guaranteed by the *discrete maximum principle* (DMP):

$$f \geq 0 \quad \text{in } \Omega \quad \Rightarrow \quad \min_{\bar{\Omega}} u_h \geq \min_{\partial\Omega} u_h^-,$$

where $u_h^- = \min\{0, u_h\}$. The monotone property,

$$f \geq 0 \quad \text{in } \Omega \quad \Rightarrow \quad \min_{\bar{\Omega}} u_h \geq 0,$$

is a sufficient condition of DMP. The monotonicity can be obtained from the M-matrix condition: Let $A = (a_{ij})$ be the stiffness matrix of a linear discretization. Then, A is called a nonsingular M-matrix if $a_{ii} > 0$ for all i,

$$a_{ij} \leq 0 \quad \forall i \neq j, \quad \sum_i a_{ij} \geq 0 \quad \forall j, \quad \sum_i a_{ij} > 0 \quad \text{for some } j.$$

In this respect, the *edge-averaged finite element* (EAFE) scheme [42, 49] is monotone if the stiffness matrix of the FEMs for the Poisson equation is an M-matrix. One of important advantages of this scheme is to obtain a stable numerical solution to a convection-dominated problem even though the mesh size is not small. The other one is that the scheme needs relatively simple computation. In this research, we apply the EAFE stabilization technique to the virtual element framework.

1.2 Virtual Element Methods

The virtual element methods (VEMs) were first introduced in [12]. In this work, the authors showed a generalization of the finite element method (FEM) for the Poisson equation to general polygonal and polyhedral meshes. Study of finite elements on general polygons has been conducted [5, 8, 46]. A flexibility between finite elements in discontinuous Galerkin (DG) methods has made it possible to use polygonal meshes [29]. These approaches need the explicit equations of local approximating functions. However, the VEMs basically use non-polynomial approximation in a polygon, and any exact form of local basis functions is not needed inside of the polygon. More exactly, virtual element functions are locally defined

by a finite number of desired properties, and their existence and uniqueness are guaranteed by the solvability of certain partial differential equations. Then, even though the local virtual element functions are not polynomials, they belong to a finite-dimensional space (called a virtual element space) determined by the properties. Proper linear functionals of the local functions are chosen, and they are called *degrees of freedom*. The degrees of freedom play an important role in the VEMs because all the quantities in the VEMs should be computed by the degrees of freedom. The degrees of freedom need to satisfy the *unisolvence* in the virtual element space: If all the degrees of freedom are given as zero, the corresponding local function is identically zero. Thus, the degrees of freedom eventually include all the essential information of the local function. Using the degrees of freedom, it is also necessary to define projection operators from the virtual element space to simple spaces such as a polynomial space. With the projection operators, the local bilinear form can be approximated by an equivalent bilinear form obtainable from the degrees of freedom. More fundamental details can be found in [13].

The VEMs have been widely applied to solve various problems in recent years; convection-diffusion problems [2, 16], nonconforming approaches [4, 7], $H(\mathrm{div})$ and $H(\mathbf{curl})$-conforming virtual elements [17, 19], mixed methods [14], and biharmonic equation [4, 22]. We especially focus on developing stabilized virtual element methods for convection-dominated problems. In the journal articles [21, 23, 24], the SUPG stabilization was successfully applied to the VEMs. They presented the improved coercivity results with mesh-dependent norms. However, it is not possible to verify the discrete maximum principle, and it is known that some solutions from the SUPG approach still contain spurious oscillations. Moreover, the SUPG-VEM contains too many terms that we need to compute, which cause higher computational complexity.

In this research, we generalize the EAFE scheme to the VEMs, and call it *edge-averaged virtual element* (EAVE) method. With the EAVE method, we expect the following advantages

and results:

- We obtain a stable numerical solution to a convection-dominated problem in a polygonal mesh even though the mesh size is not small.
- The computational complexity is relatively low.
- We show an equivalence the monotonicity of this method to the M-matrix condition of the stiffness matrix of the VEMs for the Poisson equation.
- We prove error analysis of this method and obtain reasonable convergence rates from numerical experiments.

The remaining chapters are structured as follows:

- In Chapter 2, we carefully observe the main idea of the EAFE scheme [42, 49]. We see what choices of flux approximations are possible and how the EAFE scheme is derived.
- In Chapter 3, the lowest order nodal and edge virtual element spaces [3, 12, 15, 16, 19] are introduced. More importantly, we show the relation between their canonical basis functions, and will apply it to the derivation of the EAVE method in Chapter 4. The virtual bilinear form for the Poisson equation [12, 13] is an essential factor when the EAVE method is computed. Furthermore, the approximation of the right hand side [12, 13] is introduced.
- In Chapter 4, we present a flux approximation in virtual element framework. Based on the flux approximation, we derive the EAVE method and explain why this method is simple to implement. The monotone condition of the EAVE method is verified when the stiffness matrix of the VEMs for the Poisson equation is an M-matrix.
- In Chapter 5, we start from proving some estimates of the virtual bilinear forms mentioned in Chapter 4. The main estimate is to find an upper bound of the difference

between the variational bilinear form and the EAVE bilinear form. Then, we show the inf-sup condition implying the well-posedness of the EAVE discrete problem. Various analysis techniques in VEMs are applied in this case. The convergence analysis is verified at the end of this chapter.

- In Chapter 6, numerical experiments are provided. We test convection-dominated problems as well as diffusion-dominated problems. We check that numerical convergence rates from our experiments are indeed consistent with the theoretical error estimate. In the convection-dominated regime, both smooth solutions and solutions with sharp boundary layers are considered. Through this chapter, we see the effect of edge-averaged stabilization on different mesh types.

Chapter 2

Edge-Averaged Finite Element Scheme

2.1 Main Problem

We consider the convection-diffusion problem

$$\begin{aligned} -\nabla \cdot (\alpha(\mathbf{x})\nabla u + \boldsymbol{\beta}(\mathbf{x})u) &= f \quad \text{in } \Omega, \\ u &= 0 \quad \text{on } \partial\Omega, \end{aligned} \tag{2.1}$$

where $\Omega \subset \mathbb{R}^2$ is a polygonal domain and $f \in L^2(\Omega)$. We denote the flux as

$$J(u) := \alpha(\mathbf{x})\nabla u + \boldsymbol{\beta}(\mathbf{x})u.$$

Then, the weak formulation of the problem is to find $u \in H_0^1(\Omega)$ such that

$$B(u, v) = F(v), \quad \forall v \in H_0^1(\Omega), \tag{2.2}$$

where the bilinear form and the functional on the right-hand side are defined as

$$B(w,v) = \int_\Omega J(w)\cdot\nabla v\, d\mathbf{x} \quad \text{and} \quad F(v) = \int_\Omega fv\, d\mathbf{x}.$$

The inf-sup condition [37],

$$\sup_{v\in H_0^1(\Omega)} \frac{B(w,v)}{\|v\|_{H^1(\Omega)}} \geq \bar{C}_B \|w\|_{H^1(\Omega)}, \quad \forall w \in H_0^1(\Omega) \tag{2.3}$$

implies the well-posedness of the weak formulation.

We introduce the function ψ in [42, 49] satisfying

$$\nabla\psi = \alpha^{-1}\boldsymbol{\beta},$$

which allows us to have

$$J(u) = \alpha e^{-\psi}\nabla(e^{\psi}u).$$

If the function $\psi(\mathbf{x})$ is well-defined, $J(u)$ is viewed as the diffusion flux with a non-constant coefficient $\kappa(\mathbf{x}) := \alpha(\mathbf{x})e^{-\psi(\mathbf{x})}$.

Remark 2.1. *If α and $\boldsymbol{\beta}$ are constant in K, the function ψ is defined as $\psi(\mathbf{x}) = \alpha^{-1}\boldsymbol{\beta}\cdot\mathbf{x}$ and it is unique up to a constant. However, such a function $\psi(\mathbf{x})$ may not exist in K for general $\alpha(\mathbf{x})$ and $\boldsymbol{\beta}(\mathbf{x})$ if curl $(\alpha^{-1}\boldsymbol{\beta}) \neq 0$. Hence, as introduced in [49], the function ψ is locally defined on each edge E of an element (usually a triangle) by the one-dimensional relation*

$$\frac{\partial\psi_E}{\partial\boldsymbol{\tau}_E} = \frac{1}{|\boldsymbol{\tau}_E|}\alpha^{-1}(\boldsymbol{\beta}\cdot\boldsymbol{\tau}_E),$$

where $\boldsymbol{\tau}_E$ is a tangential vector for E. In practice, we use constant approximations α_E and

$\boldsymbol{\beta}_E$ for general $\alpha(\mathbf{x})$ and $\boldsymbol{\beta}(\mathbf{x})$ on each edge E, so the local function is simply obtained as $\psi_E(\mathbf{x}) = \alpha_E^{-1}\boldsymbol{\beta}_E \cdot \mathbf{x}$ (up to a constant).

Therefore, we approximate the flux $J(u)$ in an element using the locally defined function $\psi_E(\mathbf{x})$. In [42, 49], such a flux approximation in the lowest order Nédélec space is presented on triangular meshes and it is successfully applied to develop a monotone finite element scheme. In what follows, we explain its main idea on a triangulation for Ω.

2.2 Gradient and Flux Approximations

Let $\mathcal{T}_h$ be a triangulation for Ω and $V_h = \mathcal{P}_1(\mathcal{T}_h)$ be the piecewise linear standard finite element space. We assume that $\lambda_i(\mathbf{x})$ are its canonical basis functions or barycentric coordinates in $T \in \mathcal{T}_h$. We consider the Poisson equation in terms of $\rho := e^{\psi}u_h$ for $u_h \in V_h$ while introducing a new notation $H(\rho) := H(\rho(u_h)) = J(u_h)$,

$$-\nabla \cdot (\kappa \nabla \rho) = -\nabla \cdot (H(\rho)) = f, \quad \text{in } \Omega$$

with the boundary condition $\rho = 0$ on $\partial\Omega$. Then, the variational problem is to find $\rho \in H_0^1(\Omega)$ such that

$$\mathfrak{B}(\rho, v) := \int_\Omega \kappa \nabla \rho \cdot \nabla v \, d\mathbf{x} = F(v), \tag{2.4}$$

for all $v \in H_0^1(\Omega)$. The standard finite element method for the problem (2.4) is to find $\rho_h \in V_h$ such that for all $v_h \in V_h$,

$$\mathfrak{B}(\rho_h, v_h) = F(v_h).$$

However, since the function ψ may not be well-defined on $T \in \mathcal{T}_h$ for general α and $\boldsymbol{\beta}$, the direct use of the formulation (2.4) for ρ would not give a desirable result for $u_h = e^{-\psi}\rho_h$.

The flux approximation $\bar{H}_T$ (L^2-projection)

Thus, with ψ_E on each edge $E \subset \partial T$, we focus on the nodal interpolant of $\rho(u_h)$ onto V_h,

$$\rho_I := \rho(u_h)_I = (e^{\psi_E} u_h)_I = \sum_{i=1}^{3} e^{\psi_E(\mathbf{x}_i)} u_i \lambda_i,$$

where $\lambda_i(\mathbf{x})$ are the canonical basis functions in V_h. The corresponding problem is to seek $u_h \in V_h$ such that

$$\mathfrak{B}(\rho_I, v_h) = \mathfrak{B}(\rho(u_h)_I, v_h) = F(v_h)$$

for all $v_h \in V_h$. We note that the bilinear form $\mathfrak{B}(\rho_I, v_h)$ contains $H(\rho_I) = \kappa \nabla \rho_I$, and $\kappa = \alpha e^{-\psi}$ can be considered as a Hodge star map from the 1-form $\nabla \rho_I$ to the 2-form $H(\rho_I)$. It follows from computing the bilinear form on a triangle $T \in \mathcal{T}_h$ that

$$\mathfrak{B}^T(\rho_I, v_h) = \int_T \kappa \nabla \rho_I \cdot \nabla v_h \, d\mathbf{x} = \left(\frac{1}{|T|} \int_T \kappa \, d\mathbf{x} \right) \int_T \nabla \rho_I \cdot \nabla v_h \, d\mathbf{x} \tag{2.5}$$

because both $\nabla \rho_I$ and ∇v_h are constant vectors on T. In other words, we consider to directly approximate $H(\rho)$ as a constant vector denoted by $\bar{H}_T$. Indeed, the constant approximation $\bar{H}_T$ can be obtained by the L^2-projection of $H(\rho_I)$,

$$\int_T \bar{H}_T \cdot \mathbf{e}_i \, d\mathbf{x} = \int_T H(\rho_I) \cdot \mathbf{e}_i \, d\mathbf{x} = \int_T \kappa \nabla \rho_I \cdot \mathbf{e}_i \, d\mathbf{x},$$

where $\mathbf{e}_i$ for $i = 1, 2$, are the standard vectors for $\mathbb{R}^2$. From this definition, we have

$$H(\rho) \approx \bar{H}_T = \bar{\kappa}_T \nabla \rho_I, \tag{2.6}$$

where $\bar{\kappa}_T$ is the average of κ on T, which implies the same bilinear form in (2.5).

The flux approximation $\tilde{H}_T$ (L^2-projection, modified)

In this respect, we look at a different constant approximation $\tilde{H}_T$ for $H(\rho)$ obtained from

$$\int_T \kappa^{-1}\tilde{H}_T \cdot \mathbf{e}_i \, d\mathbf{x} = \int_T \kappa^{-1} H(\rho_I) \cdot \mathbf{e}_i \, d\mathbf{x} = \int_T \nabla\rho_I \cdot \mathbf{e}_i \, d\mathbf{x}.$$

Therefore, the approximation $\tilde{H}_T$ is written as

$$H(\rho) \approx \tilde{H}_T = \tilde{\kappa}_T \nabla\rho_I, \tag{2.7}$$

where $\tilde{\kappa}_T$ is the harmonic average of κ on T, and the corresponding bilinear form is denoted as

$$\tilde{\mathfrak{B}}^T(\rho_I, v_h) = \int_T \tilde{\kappa}_T \nabla\rho_I \cdot \nabla v_h \, d\mathbf{x}.$$

The approaches described in (2.6) and (2.7) may not be efficient for the problem (2.4) with the non-constant coefficient κ because it would be necessary to have the function ψ defined over T.

The flux approximation $\hat{H}_T$ (Nédélec projection)

Therefore, we approximate $H(\rho)$ in the lowest order Nédélec space whose degrees of freedom are computed on each edge $E \subset \partial T$. The local Nédélec space of the lowest order is defined as

$$\mathcal{N}_0(T) := (\mathcal{P}_0(T))^2 + \mathbf{x}^{\perp}\mathcal{P}_0(T),$$

where $\mathbf{x}^{\perp}$ is a vector satisfying $\mathbf{x} \cdot \mathbf{x}^{\perp} = 0$. That is, a local polynomial $\mathbf{p}_0^{\mathcal{N}}$ in $\mathcal{N}_0(T)$ is represented as

$$\mathbf{p}_0^{\mathcal{N}}(\mathbf{x}) = \langle a_1 + a_2 y, a_3 - a_2 x \rangle,$$

and $\mathcal{N}_0(T)$ has 3 dimensions in $\mathbb{R}^2$. The Nédélec degrees of freedom are defined as

$$\mathrm{dof}_E^{\mathcal{N}}(\mathbf{v}) = \frac{1}{|E|} \int_E \mathbf{v} \cdot \boldsymbol{\tau}_E \, ds$$

for each $E \subset \partial T$, and the canonical basis functions $\{\boldsymbol{\varphi}_{E_j}\}_{j=1}^3$ are obtained from $\mathrm{dof}_{E_i}^{\mathcal{N}}(\boldsymbol{\varphi}_{E_j}) = \delta_{ij}$ for $1 \leq i \leq 3$. Each canonical basis function can be expressed in terms of barycentric coordinates, that is,

$$\boldsymbol{\varphi}_E = \lambda_i \nabla \lambda_{i+1} - \lambda_{i+1} \nabla \lambda_i,$$

where $\boldsymbol{\tau}_E = \mathbf{x}_{i+1} - \mathbf{x}_i$ with $\mathbf{x}_4 = \mathbf{x}_1$. Then, it is straightforward to see that $\mathbf{p}_0^{\mathcal{N}} \cdot \boldsymbol{\tau}_E$ is constant on E so that

$$\mathrm{dof}_E^{\mathcal{N}}(\mathbf{p}_0^{\mathcal{N}}) = \mathbf{p}_0^{\mathcal{N}} \cdot \boldsymbol{\tau}_E.$$

Moreover, the Nédélec projection is defined as

$$\Pi^{\mathcal{N}} \mathbf{v} := \sum_{E \subset \partial T} \mathrm{dof}_E^{\mathcal{N}}(\mathbf{v}) \boldsymbol{\varphi}_E.$$

A natural approach is to use the Nédélec projection $\hat{H}_T = \Pi^{\mathcal{N}}(H(\rho))$, that is,

$$H(\rho) \approx \hat{H}_T = \sum_{E \subset \partial T} \hat{d}_E \boldsymbol{\varphi}_E,$$

where the coefficients $\hat{d}_E$ are obtained by the following equalities,

$$\hat{d}_E = \mathrm{dof}_E^{\mathcal{N}}(\hat{H}_T) = \mathrm{dof}_E^{\mathcal{N}}(H(\rho)) = \mathrm{dof}_E^{\mathcal{N}}(\kappa\nabla\rho).$$

The coefficients $\hat{d}_E$ are determined by one-dimensional integrals,

$$\hat{d}_E = \frac{1}{|E|}\int_E \kappa\nabla\rho\cdot\boldsymbol{\tau}_E\, ds,$$

but it is not easy to compute them because both κ and $\nabla\rho$ contain the function ψ_E.

The flux approximation $\hat{H}_T$ (Nédélec projection, modified)

We focus on another approximation for $H(\rho)$ in the Nédélec space,

$$H(\rho) \approx H_T = \sum_{E\subset\partial T} d_E\boldsymbol{\varphi}_E.$$

In order to find the coefficients d_E, we use the following relation,

$$\mathrm{dof}_E^{\mathcal{N}}(\kappa^{-1}H_T) = \mathrm{dof}_E^{\mathcal{N}}(\kappa^{-1}H(\rho)) = \mathrm{dof}_E^{\mathcal{N}}(\nabla\rho).$$

It may not look appropriate that $H(\rho)$ is approximated by a 1-form formula while it is a 2-form. Interestingly, the quantity $\mathrm{dof}_E^{\mathcal{N}}(\nabla\rho)$ is represented by $\delta_E(\rho) = \delta_E(e^{\psi_E}u_h)$, where δ_E means the difference between the nodal function values at the two end points of E. Hence, the continuity of e^{ψ} and u_h inside of T is not needed to be considered, and moreover we only need the function values at the vertices of T. This fact will provide an advantage in defining and evaluating a bilinear form related to the approximation H_T. As a consequence, since

$H_T \cdot \boldsymbol{\tau}_E$ is constant on E, we obtain the explicit form of the coefficients d_E,

$$d_E = \mathrm{dof}_E^{\mathcal{N}}(H_T) = H_T \cdot \boldsymbol{\tau}_E = \left(\frac{1}{|E|} \int_E \kappa^{-1} \, ds \right)^{-1} \delta_E(\rho) = \tilde{\kappa}_E \delta_E(\rho),$$

where $\tilde{\kappa}_E$ is the harmonic average of κ on E. Note that the coefficients d_E satisfy

$$\sum_{E \subset \partial T} (\tilde{\kappa}_E)^{-1} \, d_E = 0,$$

which implies that H_T belongs to a subspace of the Nédélec space of dimension 2, but H_T may not be a constant vector. If κ is constant, we get $\sum_{E \subset \partial T} d_E = 0$ so that H_T becomes a constant vector.

In conclusion, the bilinear form is defined with the approximation H_T,

$$\begin{aligned} \mathfrak{B}_{\mathcal{N}}^T(\rho, v_h) &= \int_T H_T \cdot \nabla v_h \, d\mathbf{x} = \sum_{E \subset \partial T}^{3} (H_T \cdot \boldsymbol{\tau}_E) \int_T \boldsymbol{\varphi}_E \cdot \nabla v_h \, d\mathbf{x} \\ &= \sum_{E \subset \partial T} \tilde{\kappa}_E \delta_E(\rho) \int_T \boldsymbol{\varphi}_E \cdot \nabla v_h \, d\mathbf{x}. \end{aligned} \tag{2.8}$$

We will see that the harmonic average $\tilde{\kappa}_E$ is evaluated exactly under certain conditions of the diffusion and convection coefficients α and $\boldsymbol{\beta}$.

2.3 A Monotone Finite Element Scheme

Since $H(\rho) = H(\rho(u_h)) = J(u_h)$, we use $J_T = H_T$ as the flux approximation for $J(u_h)$. More exactly, we define J_T as an element of the Nédélec space,

$$J_T := \sum_{E \subset \partial T} \tilde{\kappa}_E \delta_E(e^{\psi_E} u_h) \boldsymbol{\varphi}_E,$$

with

$$\mathrm{dof}_E^{\mathcal{N}}(J_T) = J_T \cdot \boldsymbol{\tau}_E = \tilde{\kappa}_E \delta_E(e^{\psi_E} u_h). \tag{2.9}$$

Then, the corresponding local bilinear form is defined as

$$B_{\mathcal{N}}^T(u_h, v_h) = \sum_{E \subset \partial T} \tilde{\kappa}_E \delta_E(e^{\psi_E} u_h) \int_T \boldsymbol{\varphi}_E \cdot \nabla v_h \, d\mathbf{x}.$$

However, with this bilinear form, it is not easy to decide conditions or assumptions for the monotone condition because $B_{\mathcal{N}}^T(\lambda_i, \lambda_j)$ consists of several positive and negative terms depending on the shape of T.

The following lemma [42, 49] shows an important identity under the condition that J_T is a constant vector on T. The identity introduces a new bilinear form that implies a monotone finite element scheme.

Lemma 2.1. *If J_T is a constant vector on T, then for any $v_h \in V_h$,*

$$\sum_{E \subset \partial T} (J_T \cdot \boldsymbol{\tau}_E) \int_T \boldsymbol{\varphi}_E \cdot \nabla v_h \, d\mathbf{x} = \sum_{E \subset \partial T} \omega_E^T \, (J_T \cdot \boldsymbol{\tau}_E) \, \delta_E(v_h),$$

where

$$\omega_E^T = -\int_T \nabla \lambda_i \cdot \nabla \lambda_{i+1} \, d\mathbf{x}, \quad \textit{when} \quad \boldsymbol{\tau}_E = \mathbf{x}_{i+1} - \mathbf{x}_i.$$

Proof. If J_T is a constant vector on T, $J_T \cdot \mathbf{x}$ is a linear function for $\mathbf{x} \in T$, which implies that

$$J_T \cdot \mathbf{x} = \sum_{i=1}^{3} (J_T \cdot \mathbf{x}_i) \, \lambda_i(\mathbf{x}), \quad \text{and} \quad J_T = \sum_{i=1}^{3} (J_T \cdot \mathbf{x}_i) \, \nabla \lambda_i.$$

Moreover, it follows from the definition of the Nédélec projection that

$$\sum_{E\subset\partial T} (J_T \cdot \boldsymbol{\tau}_E)\, \boldsymbol{\varphi}_E = \Pi^{\mathcal{N}} J_T = J_T.$$

Hence, we conclude that

$$\begin{aligned}
\sum_{E\subset\partial T} (J_T \cdot \boldsymbol{\tau}_E) \int_T \boldsymbol{\varphi}_E \cdot \nabla v_h \, d\mathbf{x} & \\
&= \int_T J_T \cdot \nabla v_h \, d\mathbf{x} \\
&= \int_T \left(\sum_{i=1}^{3} (J_T \cdot \mathbf{x}_i)\, \nabla \lambda_i \right) \cdot \left(\sum_{i=1}^{3} v_i \nabla \lambda_i \right) d\mathbf{x} \\
&= \sum_{i=1}^{3} \left(\int_T \nabla \lambda_i \cdot \nabla \lambda_{i+1} \, d\mathbf{x} \right) (J_T \cdot (\mathbf{x}_{i+1} - \mathbf{x}_i))\, (v_i - v_{i+1})
\end{aligned}$$

The last equality holds because $\sum_{i=1}^{3} \lambda_i = 1$ so that $\sum_{i=1}^{3} \nabla \lambda_i = \mathbf{0}$. In this case, the difference $\mathbf{x}_{i+1} - \mathbf{x}_i$ determines $\boldsymbol{\tau}_E$ on each edge $E \subset \partial T$. □

Remark 2.2. *In other words, J_T is obtained from the degrees of freedom $J_T \cdot \boldsymbol{\tau}_E$ on three edges, and the identity* (2.9) *gives*

$$\sum_{E\subset\partial T} \tilde{\kappa}_E^{-1} (J_T \cdot \boldsymbol{\tau}_E) = 0, \tag{2.10}$$

which reduces one degree of freedom in the Nédélec space on T. If we assume that J_T is constant on T, we have a simpler condition,

$$\sum_{E\subset\partial T} (J_T \cdot \boldsymbol{\tau}_E) = 0, \tag{2.11}$$

which yields the results in Lemma 2.1. This argument will be applied to the virtual element framework.

The bilinear form of the lowest order EAFE scheme is defined as

$$B_h^T(u_h, v_h) = \sum_{E \subset \partial T} \omega_E^T \tilde{\kappa}_E \delta_E(e^{\psi_E} u_h) \delta_E(v_h) \tag{2.12}$$

based on Lemma 2.1. Therefore, the discrete problem is to find $u_h \in V_h$ such that

$$\sum_{T \in \mathcal{T}_h} B_h^T(u_h, v_h) = F(v_h), \quad \forall v_h \in V_h.$$

Its solvability and error estimates are verified by the fact that

$$B^T(u_h, v_h) = B_{\mathcal{N}}^T(u_h, v_h) = B_h^T(u_h, v_h)$$

when $J(u_h)$ is constant.

The harmonic average $\tilde{\kappa}_E$ is originally expressed as

$$\tilde{\kappa}_E = \left(\frac{1}{|E|} \int_E \alpha^{-1} e^{\psi_E} \, ds \right)^{-1}.$$

In practice, the coefficients α and $\boldsymbol{\beta}$ are approximated as a constant α_E and a constant vector $\boldsymbol{\beta}_E$ on each edge $E \subset \partial T$, respectively, and the local function is given as $\psi_E(\mathbf{x}) = {\alpha_E}^{-1} \boldsymbol{\beta}_E \cdot \mathbf{x}$. Thus, the degrees of freedom in (2.9) are explicitly expressed as

$$\tilde{\kappa}_E \delta_E(e^{\psi_E} u_h) = \alpha_E \mathbb{B}({\alpha_E}^{-1} \boldsymbol{\beta}_E \cdot (\mathbf{x}_i - \mathbf{x}_{i+1})) u_{i+1} - \alpha_E \mathbb{B}({\alpha_E}^{-1} \boldsymbol{\beta}_E \cdot (\mathbf{x}_{i+1} - \mathbf{x}_i)) u_i,$$

where $\mathbb{B}(z)$ is the Bernoulli function defined as

$$\mathbb{B}(z) = \begin{cases} \dfrac{z}{e^z - 1} & z \neq 0, \\ 1 & z = 0. \end{cases} \tag{2.13}$$

2.4 Monotonicity

We check that the EAFE discretization (2.12) is monotone [49]: The stiffness matrix corresponding to the bilinear form, $A_{ij} = B_h^T(\lambda_j, \lambda_i)$, is an M-matrix for any continuous functions $\alpha > 0$ and $\boldsymbol{\beta}$ if and only if the stiffness matrix for the Poisson equation is an M-matrix. In the 2-dimensional case, the stiffness matrix for the Poisson equation is an M-matrix if and only if the sum of the angles opposite to any edge is less than or equal to π in a triangulation $\mathcal{T}_h$. The triangulation with this condition is a Delaunay triangulation. A sufficient condition for the triangulation is that all the interior angles in each triangle of the triangulation are less than or equal to $\pi/2$. A triangulation with no obtuse triangle is a very special Delaunay triangulation, but this triangulation is easily applied to an arbitrary number of dimensions.

Let N_h be the number of all the nodes in $\mathcal{T}_h$. Then, for given $j \in \{1, \ldots, N_h\}$, we have the followings:

- If the corresponding node $\mathbf{x}_i$ is a neighbor of $\mathbf{x}_j$, then

$$A_{ij} = \sum_{E \ni \mathbf{x}_j} \omega_E \tilde{\kappa}_E \delta_E(e^{\psi_E}\lambda_j)\delta_E(\lambda_i) = -\omega_E \tilde{\kappa}_E e^{\psi_E(\mathbf{x}_j)} \leq 0,$$

  where $E \ni \mathbf{x}_j$ means all the edges having $\mathbf{x}_j$ as an endpoint.

- If $\mathbf{x}_j$ has no neighboring node on the boundary, then the j-th column sum of A is zero:

$$\sum_i A_{ij} = \sum_{E \ni \mathbf{x}_j} \omega_E \tilde{\kappa}_E \delta_E(e^{\psi_E}\lambda_j)\delta_E(\sum_i \lambda_i) = \sum_{E \ni \mathbf{x}_j} \omega_E \tilde{\kappa}_E \delta_E(e^{\psi_E}\lambda_j)\delta_E(1) = 0,$$

  which implies that $A_{jj} = \sum_{i \neq j} |A_{ij}|$.

- If $\mathbf{x}_j$ has a neighboring node on the boundary, then

$$\sum_i A_{ij} > 0 \quad \text{or} \quad A_{jj} > \sum_{i \neq j} |A_{ij}|.$$

Chapter 3

Virtual Element Methods

3.1 Virtual Element Spaces

Let us define $\mathcal{K}_h$ as a decomposition of the polygonal domain Ω into convex polygonal elements K for a given mesh size h. We assume that each element K satisfies the shape regularity presented in [26, 33]. On an element K, we denote $\mathbf{x}_i$ as a vertex for $1 \leq i \leq N_V$ and E_j as an edge for $1 \leq j \leq N_E$, where N_V is the number of vertices and N_E is that of edges. We also define a tangential vector or a vector between consecutive vertices as $\boldsymbol{\tau}_j = \mathbf{x}_{j+1} - \mathbf{x}_j$ for $1 \leq j \leq N_E$ with $j+1$ modulo N_V. For a simple polygon, $N_V = N_E$. We label the indices of the vertices or edges counterclockwise.

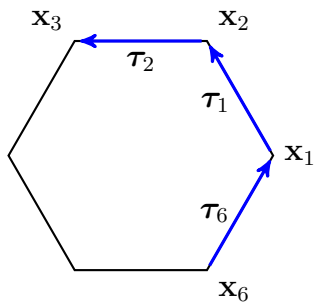

Figure 3.1: A numbering of vertices and edges in a polygon.

3.1.1 The lowest order nodal virtual element spaces

We first introduce the basic lowest order local nodal space presented in [12, 13]. A function space is defined to have some conditions on the boundary edges of K,

$$B_1(\partial K) := \left\{ v_h \in \mathcal{C}^0(\partial K) : v_h|_E \in \mathcal{P}_1(E),\ \forall E \subset \partial K \right\}.$$

The standard nodal virtual element space $V_1(K)$

Then, the local nodal space [12, 13] is defined as

$$V_1(K) = \left\{ v_h \in H^1(K) : v_h|_{\partial K} \in B_1(\partial K),\ \Delta v_h|_K = 0 \right\},$$

and the degrees of freedom are given as the values of v_h at the vertices of K, i.e.,

$$\mathrm{dof}_i(v_h) = v_h(\mathbf{x}_i), \tag{3.1}$$

for $1 \le i \le N_V$.

It is immediate to see that the dimension of $V_1(K)$ is N_V, and it is the same as the number of the degrees of freedom. Also, the canonical basis in K, $\{\phi_j\}_{j=1}^{N_V}$, is chosen by $\mathrm{dof}_i(\phi_j) = \delta_{ij}$. The important proposition that the degrees of freedom are *unisolvent* for $V_1(K)$ is easily proved [12]. Indeed, if we assume that all the degrees of freedom (3.1) are zero, then $v_h \equiv 0$ on ∂K so that by the integration by parts,

$$\int_K |\nabla v_h|^2 \, d\mathbf{x} = \int_{\partial K} (\nabla v_h \cdot \mathbf{n})\, v_h \, ds - \int_K (\Delta v_h)\, v_h \, d\mathbf{x} = 0,$$

where $\mathbf{n}$ is the outward normal vector on ∂K. Thus, we conclude that v_h is constant in K so that the zero boundary condition on ∂K implies $v_h \equiv 0$ in K.

Since we do not know the explicit equation of v_h in K, it would not be possible to exactly compute a bilinear form including any functions in $V_1(K)$. However, we will define an equivalent bilinear form that can be exactly evaluated by the given degrees of freedom. We now introduce a proper projection operator evaluated by the degrees of freedom and use it to define the equivalent bilinear form. The basic choice presented in [12, 13] is the local H^1-projection operator, that is, $\Pi_1^\nabla : V_1(K) \to \mathcal{P}_1(K)$ with

$$\int_K \left(\nabla \Pi_1^\nabla v_h - \nabla v_h\right) \cdot \nabla p_1 \, d\mathbf{x} = 0, \quad \forall p_1 \in \mathcal{P}_1(K), \tag{3.2}$$

$$\frac{1}{N_V} \sum_{i=1}^{N_V} \left(\Pi_1^\nabla v_h(\mathbf{x}_i) - v_h(\mathbf{x}_i)\right) = 0. \tag{3.3}$$

In the condition (3.2), the following quantity can be exactly computed by the degrees of freedom,

$$\int_K \nabla v_h \cdot \nabla p_1 \, d\mathbf{x} = \int_{\partial K} (\nabla p_1 \cdot \mathbf{n}) \, v_h \, ds = \sum_{E \subset \partial K} (\nabla p_1 \cdot \mathbf{n}_E) \int_E v_h \, ds$$

because ∇p_1 is a constant vector and $\Delta p_1 \equiv 0$ in K. The second condition (3.3) determines the constant term of the linear polynomial $\Pi_1^\nabla v_h$. Furthermore, if we denote $\mathbf{\Pi}_0^0$ as the local L^2-projection onto the constant vector field $(\mathcal{P}_0(K))^2$, we have $\mathbf{\Pi}_0^0 \nabla v_h = \nabla \Pi_1^\nabla v_h$. More exactly, it follows from their definitions that

$$\int_K \nabla \Pi_1^\nabla v_h \cdot \nabla p_1 \, d\mathbf{x} = \int_K \nabla v_h \cdot \nabla p_1 \, d\mathbf{x} = \int_K \mathbf{\Pi}_0^0 \nabla v_h \cdot \nabla p_1 \, d\mathbf{x}.$$

Now, we focus on finding an explicit formula for the projections. For any $v_h \in V_1(K)$, the linearity of the operator ∇ implies that $\mathbf{\Pi}_0^0 \nabla v_h$ is determined by $\mathbf{\Pi}_0^0 \nabla \phi_i$ for $1 \le i \le N_V$.

Let $\mathbf{\Pi}_0^0 \nabla \phi_i = \langle q_i^1, q_i^2 \rangle = q_i^1 \mathbf{e}_1 + q_i^2 \mathbf{e}_2$. Then, by the integration by parts, we have

$$\begin{aligned} q_i^1 |K| &= \int_K \nabla \phi_i \cdot \mathbf{e}_1 \, d\mathbf{x} = \sum_{j=1}^{N_E} \int_{E_j} \phi_i \left(\mathbf{e}_1 \cdot \mathbf{n}_j \right) \, ds \\ &= n_{i-1}^1 \int_{E_{i-1}} \phi_i \, ds + n_i^1 \int_{E_i} \phi_i \, ds \\ &= \frac{1}{2} |E_{i-1}| n_{i-1}^1 + \frac{1}{2} |E_i| n_i^1 \\ &= \frac{1}{2} (y_{i+1} - y_{i-1}), \end{aligned}$$

where $\mathbf{n}_j = \langle n_j^1, n_j^2 \rangle = \langle y_{j+1} - y_j, -(x_{j+1} - x_j) \rangle / |E_j|$ is the outward unit normal vector on the edge E_j for $1 \le j \le N_E$. Similarly, we obtain

$$q_i^2 |K| = \frac{1}{2} |E_{i-1}| n_{i-1}^2 + \frac{1}{2} |E_i| n_i^2 = -\frac{1}{2} (x_{i+1} - x_{i-1}).$$

Hence, $\mathbf{\Pi}_0^0 \nabla \phi_i$ can be geometrically viewed as the average of the two outward normal vectors

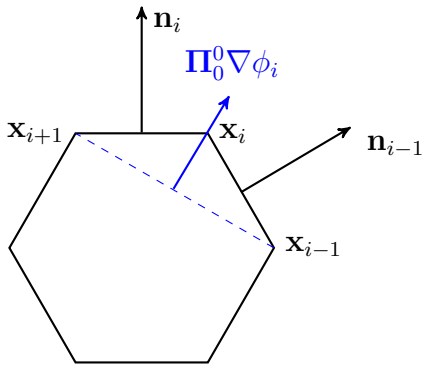

on the two adjacent edges to $\mathbf{x}_i$, or the outward vector perpendicular to the line segment between $\mathbf{x}_{i+1}$ and $\mathbf{x}_{i-1}$ with different scales. From this result and the condition (3.3), we finally have

$$\Pi_1^\nabla \phi_i = (\mathbf{\Pi}_0^0 \nabla \phi_i) \cdot (\mathbf{x} - \mathbf{x}_K) + \frac{1}{N_V},$$

and the linear combination of v_h gives

$$\Pi_1^\nabla v_h = (\boldsymbol{\Pi}_0^0 \nabla v_h) \cdot (\mathbf{x} - \mathbf{x}_K) + \frac{1}{N_V} \sum_{i=1}^{N_V} v_h(\mathbf{x}_i),$$

where

$$\mathbf{x}_K = \frac{1}{N_V} \sum_{i=1}^{N_V} \mathbf{x}_i$$

is the barycenter of K.

In summary, the local nodal space $V_1(K)$ satisfies the following conditions:

- the dimension of $V_1(K)$ is N_V.
- the degrees of freedom (3.1) are unisolvent for $V_1(K)$.
- $\mathcal{P}_1(K) \subset V_1(K)$.
- the H^1-projection Π_1^∇ is computable by the degrees of freedom of $V_1(K)$.

A modified nodal virtual element space $\bar{V}_1(K)$ dealing with L^2-projection

We are interested in the L^2-projection operator Π_1^0 onto $\mathcal{P}_1(K)$ defined by

$$\int_K \left(\Pi_1^0 v_h - v_h\right) p_1 \, d\mathbf{x}, \quad \forall p_1 \in \mathcal{P}_1(K).$$

Then, we encounter a problem about how we compute

$$\int_K v_h p_1 \, d\mathbf{x}$$

using the degrees of freedom (3.1). Unfortunately, there is no way to compute it with (3.1) in $V_1(K)$. A possible solution for this problem is presented by [3, 15]. According to the ideas in [3, 15], we enlarge the local space $V_1(K)$ by changing the condition $\Delta v_h|_K = 0$. For example, if $\Delta v_h|_K$ is considered as a constant, the dimension of such a local space is $N_V + 1$ and one more degree of freedom needed to fill out the dimension is

$$\int_K v_h \, d\mathbf{x}. \tag{3.4}$$

Thus, it is possible to obtain $\Pi_0^0 v_h$ from the degrees of freedom (3.1) and (3.4). In general, if $\Delta v_h|_K \in \mathcal{P}_1(K)$, the natural degrees of freedom are

$$\int_K v_h p_1 \, d\mathbf{x}, \quad \forall p_1 \in \mathcal{P}_1(K), \tag{3.5}$$

so we can get the L^2-projection of v_h of order up to k.

However, the additional degrees of freedom (3.5) would cause higher computational costs. Hence, by adding proper conditions to the space $V_1(K)$, the degrees of freedom (3.5) are can be eliminated. We introduce the modified local nodal virtual space of the lowest order $k = 1$ [3],

$$\bar{V}_1(K) = \big\{ v_h \in H^1(K) : v_h|_{\partial K} \in B_1(\partial K),\ \Delta v_h \in \mathcal{P}_1(K), \\ (v_h - \Pi_1^\nabla v_h, p_1)_{L^2(K)} = 0,\ \forall p_1 \in \mathcal{P}_1(K) \big\}.$$

The definition of the modified space with a general number k is presented in [3]. In this case, we already computed the polynomial $\Pi_1^\nabla v_h$ using the degrees of freedom (3.1), and the additional degrees of freedom (3.5) are given by $\Pi_1^\nabla v_h$. Therefore, the space $\bar{V}_1(K)$ satisfies the followings:

- the dimension of $\bar{V}_1(K)$ is N_V.

- the degrees of freedom (3.1) are unisolvent for $\bar{V}_1(K)$.
- $\mathcal{P}_1(K) \subset \bar{V}_1(K)$.
- the H^1-projection Π_1^∇ and the L^2-projection Π_1^0 are computable by the degrees of freedom of $\bar{V}_1(K)$, and moreover $\Pi_1^\nabla = \Pi_1^0$ in $\bar{V}_1(K)$.

Indeed, the second condition is satisfied because if the degrees of freedom (3.1) are zero, we see $\Pi_1^\nabla v_h \equiv 0$ in K so that

$$\int_K (\Delta v_h)\, v_h \, d\mathbf{x} = \int_K (\Delta v_h)\, \Pi_1^0 v_h \, d\mathbf{x} = 0.$$

In this case, the first equality holds because $\Delta v_h \in \mathcal{P}_1(K)$, and the second comes from the identity $\Pi_1^\nabla v_h = \Pi_1^0 v_h$ in $\bar{V}_1(K)$. We note that $\Pi_k^\nabla v_h \neq \Pi_k^0 v_h$ if $k > 1$ (See details in [3]).

A reduced nodal virtual element space $\hat{V}_1(K)$

We will look at a different idea to get a reduced local nodal space. If we assume that any given polynomial $p_k \in \mathcal{P}_k(K)$ is written as $p_k(\mathbf{x}) = \mathrm{div}((\mathbf{x} - \mathbf{x}_K)q_k)$ for some $q_k \in \mathcal{P}_k(K)$, then we have

$$\int_K v_h p_k \, d\mathbf{x} = \int_{\partial K} ((\mathbf{x} - \mathbf{x}_K) \cdot \mathbf{n})\, v_h q_k \, ds - \int_K (\nabla v_h \cdot (\mathbf{x} - \mathbf{x}_K))\, q_k \, d\mathbf{x}.$$

On the right hand side, the first term can be obtained by the degrees of freedom at the vertices (3.1), and the second term can be considered as additional degrees of freedom that correspond to (3.5). Thus, as a simple case, we define a local nodal virtual element space enlarged from $V_1(K)$

$$\tilde{V}_1(K) = \left\{ v_h \in H^1(K) : v_h|_{\partial K} \in B_1(\partial K),\ \Delta v_h \in \mathcal{P}_0(K) \right\}.$$

Including the degrees of freedom (3.1), an equivalent degree of freedom to (3.4),

$$\int_K \nabla v_h \cdot (\mathbf{x} - \mathbf{x}_K)\, d\mathbf{x}, \tag{3.6}$$

fills out the dimension of $\tilde{V}_1(K)$. It is clear to check that all the degrees of freedom (3.1) and (3.6) are unisolvent for $\tilde{V}_1(K)$. If the degrees of freedom are zero, then $v_h = 0$ on ∂K and $\int_K v_h\, d\mathbf{x} = 0$, which implies that $v_h \equiv 0$ in K.

The next step is to reduce the dimension of the space $\tilde{V}_1(K)$ by adding a proper restriction. Thus, we define a reduced local nodal virtual space and only consider the degrees of freedom (3.1) in the reduced space. Most importantly, when the dimension of $\tilde{V}_1(K)$ is reduced, the reduced space must contain $\mathcal{P}_1(K)$. It is easy to see that

$$\int_K \nabla p_1 \cdot (\mathbf{x} - \mathbf{x}_K)\, d\mathbf{x} = 0, \quad \forall p_1 \in \mathcal{P}_1(K).$$

Therefore, the reduced local nodal space in [20] is defined as

$$\hat{V}_1(K) = \left\{ v_h \in H^1(K) : v_h|_{\partial K} \in B_1(\partial K),\ \Delta v_h \in \mathcal{P}_0(K),\ (\nabla v_h, \mathbf{x} - \mathbf{x}_K)_{L^2(K)} = 0 \right\}.$$

Then, the space $\hat{V}_1(K)$ satisfies the following conditions:

- the dimension of $\hat{V}_1(K)$ is N_V.
- the degrees of freedom (3.1) are unisolvent for $\hat{V}_1(K)$.
- $\mathcal{P}_1(K) \subset \hat{V}_1(K)$.
- the H^1-projection Π_1^∇ and the L^2-projection Π_0^0 are computable by the degrees of freedom of $\hat{V}_1(K)$.

The global nodal virtual element spaces

For the local virtual element spaces $V_1(K)$, $\bar{V}_1(K)$, and $\hat{V}_1(K)$, the global spaces are defined in the same way [12, 13] because they include the same degrees of freedom. For example, we define the global space for $V_1(K)$,

$$V_1(\mathcal{K}_h) := \left\{ v_h \in H_0^1(\Omega) : v_h|_K \in V_1(K),\ \forall K \in \mathcal{K}_h \right\}.$$

The global degrees of freedom are all the values of v_h at the internal vertices of the decomposition $\mathcal{K}_h$.

3.1.2 The lowest order local edge virtual element spaces

The general definition of local edge virtual element spaces are presented in [17, 19]. Here, we introduce some lowest order edge spaces and explain important conditions. We consider two different local edge spaces,

$$\mathbf{V}_0(K) = \left\{ \mathbf{v}_h \in (L^2(K))^2 : \operatorname{div} \mathbf{v}_h = 0,\ \operatorname{rot} \mathbf{v}_h \in \mathcal{P}_0(K), \right.$$
$$\left. \mathbf{v}_h \cdot \boldsymbol{\tau}_E \in \mathcal{P}_0(E),\ \forall E \subset \partial K \right\},$$

and

$$\bar{\mathbf{V}}_0(K) = \left\{ \mathbf{v}_h \in (L^2(K))^2 : \operatorname{div} \mathbf{v}_h \in \mathcal{P}_0(K),\ \operatorname{rot} \mathbf{v}_h \in \mathcal{P}_0(K), \right.$$
$$\left. \mathbf{v}_h \cdot \boldsymbol{\tau}_E \in \mathcal{P}_0(E),\ \forall E \subset \partial K \right\}.$$

Existence of local edge virtual element functions

We check the existence of such functions $\mathbf{v}_h \in \bar{\mathbf{V}}_0(K)$, that is, we find $\mathbf{v}_h \in (L^2(K))^2$ satisfying all the conditions in $\bar{\mathbf{V}}_0(K)$. The existence of such $\mathbf{v}_h \in \mathbf{V}_0(K)$ is also proved in the same way. For more details, one can see [6]. Let us define the following spaces

$$G(K) := \left\{\nabla\varphi \mid \varphi \in H^1(K)\right\}, \quad G_0(K) := \left\{\nabla\varphi \mid \varphi \in H_0^1(K)\right\},$$

and

$$R(K) := \left\{\mathbf{rot}\ \xi \mid \xi \in H^1(K)\right\}, \quad R_0(K) := \left\{\mathbf{rot}\ \xi \mid \xi \in H_0^1(K)\right\}.$$

Then, it follows from Theorem 3 of [6] that

$$(L^2(K))^2 = G(K) \oplus R_0(K) = G_0(K) \oplus R(K).$$

For any $\mathbf{v}_h \in (L^2(K))^2$, $\mathbf{v}_h$ can be written as a Helmholtz decomposition, that is, $\mathbf{v}_h = \nabla\varphi + \mathbf{rot}\ \xi$ for some $\varphi \in H_0^1(K)$ and $\xi \in H^1(K)$ (or for some $\varphi \in H^1(K)$ and $\xi \in H_0^1(K)$). We consider the following problem related to the conditions in $\bar{\mathbf{V}}_0(K)$,

$$\begin{cases} \text{div } \mathbf{v}_h = \rho_d, & \text{in } K, \\ \text{rot } \mathbf{v}_h = \rho_r, & \text{in } K, \\ \mathbf{v}_h \cdot \boldsymbol{\tau}_E = \rho_E, & \text{on } E \subset \partial K, \end{cases}$$

where ρ_d, ρ_r, and ρ_E are given constants in $\bar{\mathbf{V}}_0(K)$. Hence, the first equation implies the Poisson problem,

$$\Delta\varphi = \rho_d \quad \text{in } K,$$

with the boundary condition $\varphi = 0$ on K, and the second equation gives

$$\text{rot } \mathbf{v}_h = \text{rot } (\mathbf{rot}\ \xi) = -\Delta\xi = \rho_r.$$

It follows from $\nabla\varphi \cdot \boldsymbol{\tau}_E = 0$ on $E \subset \partial K$ that

$$\mathbf{v}_h \cdot \left(\frac{\boldsymbol{\tau}_E}{|\boldsymbol{\tau}_E|}\right) = \mathbf{rot}\ \xi \cdot \left(\frac{\boldsymbol{\tau}_E}{|\boldsymbol{\tau}_E|}\right) = \nabla\xi \cdot \mathbf{n}_E = \rho_E/|E|,$$

which is the Neumann boundary condition for the Poisson problem with respect to ξ. In this case, the comparability condition,

$$\int_K \rho_r \, d\mathbf{x} = \sum_{E\subset\partial K} \frac{1}{|E|} \int_E \rho_E \, ds,$$

must be satisfied for the existence of such a function ξ, and it will be easily verified by the integration by parts.

Degrees of freedom

We take a look at degrees of freedom for $\mathbf{V}_0(K)$ and $\bar{\mathbf{V}}_0(K)$. The natural degrees of freedom in [17, 18, 19, 20] are

$$\text{dof}_E(\mathbf{v}_h) = \frac{1}{|E|} \int_E \mathbf{v}_h \cdot \boldsymbol{\tau}_E \, ds, \tag{3.7}$$

for each $E \subset \partial K$. In addition, since the quantity rot $\mathbf{v}_h$ is assumed as a constant on each element K in the spaces $\mathbf{V}_0(K)$ and $\bar{\mathbf{V}}_0(K)$, we obtain from the integration by parts,

$$\begin{aligned} |K|\,(\text{rot } \mathbf{v}_h) &= \int_K \text{rot } \mathbf{v}_h \, d\mathbf{x} \\ &= \sum_{E\subset\partial K} \int_E \mathbf{v}_h \cdot \left(\frac{\boldsymbol{\tau}_E}{|\boldsymbol{\tau}_E|} \right) ds \\ &= \sum_{E\subset\partial K} \frac{1}{|E|} \int_E \mathbf{v}_h \cdot \boldsymbol{\tau}_E \, ds. \end{aligned} \tag{3.8}$$

We note that the second equality guarantees the comparability condition, and we also see that rot $\mathbf{v}_h$ is exactly computed by the degrees of freedom (3.7).

While the dimension of $\mathbf{V}_0(K)$ is N_E, the dimension of $\bar{\mathbf{V}}_0(K)$ is $N_E + 1$. This is because the value ρ_d can be arbitrarily chosen as a constant in $\bar{\mathbf{V}}_0(K)$ while ρ_d is fixed as zero in $\mathbf{V}_0(K)$. Thus, we need one more degree of freedom to fill out the dimension of $\bar{\mathbf{V}}_0(K)$. The additional degree of freedom is used to show that all given degrees of freedom are unisolvent for $\bar{\mathbf{V}}_0(K)$. Indeed, for any $\mathbf{v}_h \in \bar{\mathbf{V}}_0(K)$, we write div $\mathbf{v}_h = \text{div}((\mathbf{x} - \mathbf{x}_K)p_0)$ for some $p_0 \in \mathcal{P}_0(K)$ because div $\mathbf{v}_h$ is a constant. Then, it follows from $\text{div}(\mathbf{v}_h - (\mathbf{x} - \mathbf{x}_K)p_0) = 0$ that

$$\mathbf{v}_h = \mathbf{rot}\ \zeta + (\mathbf{x} - \mathbf{x}_K)p_0,$$

for some differentiable function ζ. This identity and the integration by parts imply that

$$\begin{aligned} \int_K |\mathbf{v}_h|^2 \, d\mathbf{x} &= \int_K \mathbf{v}_h \cdot (\mathbf{rot}\ \zeta + (\mathbf{x} - \mathbf{x}_K)\, p_0) \\ &= \int_K (\text{rot } \mathbf{v}_h)\, \zeta \, d\mathbf{x} - \sum_{E\subset\partial K} \frac{1}{|E|} \int_E (\mathbf{v}_h \cdot \boldsymbol{\tau}_E)\, \zeta \, ds + \int_K \mathbf{v}_h \cdot (\mathbf{x} - \mathbf{x}_K)\, p_0 \, d\mathbf{x}. \end{aligned}$$

As you see here, the first two terms are vanished when the degrees of freedom at (3.7) are

zero, so the additional degree of freedom is determined as

$$\int_K \mathbf{v}_h \cdot (\mathbf{x} - \mathbf{x}_K)\, d\mathbf{x}. \tag{3.9}$$

Thus, if this degree of freedom is also zero, we finally get $\mathbf{v}_h \equiv 0$ in K. From the above arguments, it is easy to prove that the degrees of freedom (3.7) are unisolvent for $\mathbf{V}_0(K)$. Indeed, since div $\mathbf{v}_h = 0$, $\mathbf{v}_h = \mathbf{rot}\ \zeta$ for some function ζ, so $\int_K |\mathbf{v}_h|^2\ d\mathbf{x} = 0$ when the degrees of freedom (3.7) are zero.

L^2-projection $\mathbf{\Pi}_1^0$

The polynomial space $(\mathcal{P}_1(K))^2$ is decomposed into

$$(\mathcal{P}_1(K))^2 = \mathbf{rot}\ \mathcal{P}_2(K) + \mathbf{x}\mathcal{P}_0(K).$$

The L^2-projection $\mathbf{\Pi}_1^0 : \bar{\mathbf{V}}_0(K) \to (\mathcal{P}_1(K))^2$ is computed as

$$\begin{aligned}
\int_K \mathbf{\Pi}_1^0 \mathbf{v}_h \cdot \mathbf{p}_1\, d\mathbf{x} &= \int_K \mathbf{v}_h \cdot \mathbf{p}_1\, d\mathbf{x} \\
&= \int_K \mathbf{v}_h \cdot (\mathbf{rot}\ p_2 + (\mathbf{x} - \mathbf{x}_K)\, p_0)\, d\mathbf{x} \\
&= \int_K (\mathrm{rot}\ \mathbf{v}_h)\, p_2\, d\mathbf{x} - \sum_{E \subset \partial K} \frac{1}{|E|} \int_E (\mathbf{v}_h \cdot \boldsymbol{\tau}_E)\, p_2\, ds \\
&\qquad + p_0 \int_K \mathbf{v}_h \cdot (\mathbf{x} - \mathbf{x}_K)\, d\mathbf{x}.
\end{aligned}$$

The right hand side can be evaluated by the degrees of freedom (3.7) and (3.9). We note that it is possible to compute only the L^2-projection $\mathbf{\Pi}_0^0 : \mathbf{V}_0(K) \to (\mathcal{P}_0(K))^2$ with the degrees of freedom (3.7).

Summary of properties of $\mathbf{V}_0(K)$ and $\bar{\mathbf{V}}_0(K)$

The space $\mathbf{V}_0(K)$ satisfies the following conditions:

- the dimension of $\mathbf{V}_0(K)$ is N_E.
- the degrees of freedom (3.7) are unisolvent for $\mathbf{V}_0(K)$.
- $(\mathcal{P}_0(K))^2 \subset \mathbf{V}_0(K)$.
- the L^2-projection $\mathbf{\Pi}_0^0$ are computable by the degrees of freedom of $\mathbf{V}_0(K)$.

We also summarize the important properties of $\bar{\mathbf{V}}_0(K)$:

- the dimension of $\bar{\mathbf{V}}_0(K)$ is $N_E + 1$.
- the degrees of freedom (3.7) and (3.9) are unisolvent for $\bar{\mathbf{V}}_0(K)$.
- $(\mathcal{P}_0(K))^2 \subset \bar{\mathbf{V}}_0(K)$.
- the L^2-projection $\mathbf{\Pi}_1^0$ are computable by the degrees of freedom of $\bar{\mathbf{V}}_0(K)$.

A reduced edge virtual element space $\hat{\mathbf{V}}_0(K)$

We introduce an idea to reduce the dimension of $\bar{\mathbf{V}}_0(K)$. It comes from the required condition that $(\mathcal{P}_0(K))^2 \subset \bar{\mathbf{V}}_0(K)$. To be specific, we look at

$$\int_K \mathbf{p}_0 \cdot (\mathbf{x} - \mathbf{x}_K)\, d\mathbf{x} = 0, \quad \forall \mathbf{p}_0 \in (\mathcal{P}_0(K))^2,$$

so the reduced local virtual edge space in [20] is

$$\hat{\mathbf{V}}_0(K) = \big\{\mathbf{v}_h \in (L^2(K))^2 \mid \text{div } \mathbf{v}_h \in \mathcal{P}_0(K),\ \text{rot } \mathbf{v}_h \in \mathcal{P}_0(K),\\ \mathbf{v}_h \cdot \boldsymbol{\tau}_E \in \mathcal{P}_0(E),\ \forall E \subset \partial K,\ (\mathbf{v}_h, \mathbf{x} - \mathbf{x}_K)_{L^2(K)} = 0\big\}.$$

In conclusion, it is easy to check the properties of the space $\hat{\mathbf{V}}_0(K)$:

- the dimension of $\hat{\mathbf{V}}_0(K)$ is N_E.
- the degrees of freedom (3.7) are unisolvent for $\hat{\mathbf{V}}_0(K)$.
- $(\mathcal{P}_0(K))^2 \subset \hat{\mathbf{V}}_0(K)$.
- the L^2-projection $\boldsymbol{\Pi}_1^0$ are computable by the degrees of freedom of $\hat{\mathbf{V}}_0(K)$.

Canonical basis with respect to the degrees of freedom

Let $\{\boldsymbol{\chi}_j\}_{j=1}^{N_E}$ be the canonical basis of $\mathbf{V}_0(K)$ (or $\hat{\mathbf{V}}_0(K)$), that is, with the degrees of freedom (3.7)

$$\text{dof}_{E_i}(\boldsymbol{\chi}_j) = \frac{1}{|E_i|}\int_{E_i} \boldsymbol{\chi}_j \cdot \boldsymbol{\tau}_i\, ds = \boldsymbol{\chi}_j \cdot \boldsymbol{\tau}_i = \delta_{ij},$$

where $\boldsymbol{\tau}_i = \mathbf{x}_{i+1} - \mathbf{x}_i$ for $1 \le i \le N_E$. Then, any vector function $\mathbf{v}_h \in \mathbf{V}_0(K)$ is written as

$$\mathbf{v}_h = \sum_{E \subset \partial K} (\mathbf{v}_h \cdot \boldsymbol{\tau}_E)\, \boldsymbol{\chi}_E \quad \text{or} \quad \sum_{i=1}^{N_E} (\mathbf{v}_h \cdot \boldsymbol{\tau}_i)\, \boldsymbol{\chi}_i.$$

The global edge virtual element spaces

The global edge virtual element spaces are required to preserve the $H(\mathbf{curl})$-conformity [18, 19, 20]. For the local virtual element space $\mathbf{V}_0(K)$, the global space in 2 dimensions is

defined as

$$\mathbf{V}_0(\mathcal{K}_h) := \{\mathbf{v}_h \in H_0(\mathrm{rot};\Omega) : \mathbf{v}_h|_K \in \mathbf{V}_0(K),\ \forall K \in \mathcal{K}_h\}\,.$$

The global space corresponding to $\hat{\mathbf{V}}_0(K)$ is defined in the same way. Their global degrees of freedom are $\mathbf{v}_h \cdot \boldsymbol{\tau}_E$ for all interior edges of the decomposition $\mathcal{K}_h$. Moreover, the global space for $\bar{\mathbf{V}}_0(K)$ needs additional global degrees of freedom $\int_K \mathbf{v}_h \cdot (\mathbf{x} - \mathbf{x}_K)\, d\mathbf{x}$ for all $K \in \mathcal{K}_h$.

3.1.3 Relations between $V_1(K)$ and $\mathbf{V}_0(K)$

We present important relations between the local nodal space $V_1(K)$ and the local edge space $\mathbf{V}_0(K)$. These relations allow us to derive an efficient flux approximation in virtual element framework.

Proposition 3.1. *$\nabla V_1(K)$ is a subset of $\mathbf{V}_0(K)$, and moreover*

$$\nabla V_1(K) = \{\mathbf{v}_h \in \mathbf{V}_0(K) \mid \mathrm{rot}\ \mathbf{v}_h = 0\}\,.$$

Proof. For any local function $v_h \in V_1(K)$, it is easy to check that $\mathrm{div}\,(\nabla v_h) = 0$, $\mathrm{rot}\,(\nabla v_h) = 0$, and $\nabla v_h \cdot \boldsymbol{\tau}_E \in \mathcal{P}_0(E)$ for every $E \subset \partial K$. Thus, we have $\nabla v_h \in \mathbf{V}_0(K)$, so

$$\nabla V_1(K) \subset \{\mathbf{v}_h \in \mathbf{V}_0(K) \mid \mathrm{rot}\ \mathbf{v}_h = 0\}\,.$$

Now, both are finite dimensional spaces, and

$$\begin{aligned}\dim(\nabla V_1(K)) &= \dim(V_1(K)) - 1 = \dim(\mathbf{V}_0(K)) - 1\\ &= \dim(\{\mathbf{v}_h \in \mathbf{V}_0(K) \mid \mathrm{rot}\ \mathbf{v}_h = 0\})\,.\end{aligned}$$

□

This proof is similar to the arguments in [20] showing the same relation between $\hat{V}_1(K)$ and $\hat{\mathbf{V}}_0(K)$, i.e.,

$$\nabla \hat{V}_1(K) = \left\{ \mathbf{v}_h \in \hat{\mathbf{V}}_0(K) \mid \text{rot } \mathbf{v}_h = 0 \right\}.$$

Then, we verify the relation between the canonical basis functions, $\{\phi_i\}_{i=1}^{N_V}$ and $\{\boldsymbol{\chi}_j\}_{j=1}^{N_E}$.

Lemma 3.1. *In the space* $\mathbf{V}_0(K)$ *(or* $\hat{\mathbf{V}}_0(K)$*), we have*

$$\boldsymbol{\chi}_n - \boldsymbol{\chi}_m = -\sum_{l=m+1}^{n} \nabla \phi_l.$$

for $1 \leq m < n \leq N_E$.

Proof. Let $\mathbf{w}_h = -\sum_{l=m+1}^{n} \nabla \phi_l$. Then, $\mathbf{w}_h \in \nabla V_1(K) \subset \mathbf{V}_0(K)$ by Proposition 3.1. It is clear to see that

$$\text{dof}_E(\mathbf{w}_h) = \text{dof}_E(\boldsymbol{\chi}_n - \boldsymbol{\chi}_m),$$

for all $E \subset \partial K$. Therefore, $\mathbf{w}_h = \boldsymbol{\chi}_n - \boldsymbol{\chi}_m$ in $\mathbf{V}_0(K)$ by the unisolvent condition. □

3.2 Virtual Bilinear Forms for the Poisson Equation

We introduce bilinear forms appearing in virtual element methods for the Poisson equation. These bilinear forms will be applied to construct the edge-averaged virtual element scheme. The classic local bilinear form for the Poisson equation is denoted as

$$a^K(u, v) = \int_K \nabla u \cdot \nabla v \, d\mathbf{x}.$$

Since we do not know the explicit forms of $u_h, v_h \in V_1(K)$ inside K, it would not be possible to exactly compute $a^K(u_h, v_h)$. Therefore, we use the equivalent bilinear form in [12, 13]

$$a_h^K(u_h, v_h) = \int_K \nabla \Pi_1^\nabla u_h \cdot \nabla \Pi_1^\nabla v_h \, d\mathbf{x} + S^K(u_h - \Pi_1^\nabla u_h, v_h - \Pi_1^\nabla v_h). \tag{3.10}$$

for all $u_h, v_h \in V_1(K)$. In this case, the stabilization term S^K will be chosen to verify that there are positive constants c_0 and c_1 independent of h_K such that

$$c_0 a^K(v_h, v_h) \leq S^K(v_h, v_h) \leq c_1 a^K(v_h, v_h),$$

for every $v_h \in V_1(K)$ with $\Pi_1^\nabla v_h = 0$. These inequalities directly imply the norm equivalence,

$$\gamma_* a^K(v_h, v_h) \leq a_h^K(v_h, v_h) \leq \gamma^* a^K(v_h, v_h), \quad \forall v_h \in V_1(K), \tag{3.11}$$

for some positive constants γ_* and γ^* independent of h_K. (See [12, 13] for details.) Here, we introduce the most popular choice for S^K,

$$S_\mathcal{V}^K(u_h, v_h) := \sum_{i=1}^{N_V} \mathrm{dof}_i(u_h)\mathrm{dof}_i(v_h). \tag{3.12}$$

Let $\mathbf{\Pi}^\nabla = (\mathbf{\Pi}^\nabla)_{ri}$ be the matrix corresponding to the H^1-projection, that is, $(\mathbf{\Pi}^\nabla)_{ri} = \mathrm{dof}_r(\Pi^\nabla \phi_i)$. Then, the matrix corresponding to the stabilization term

$$S_\mathcal{V}^K(\phi_j - \Pi_1^\nabla \phi_j, \phi_i - \Pi_1^\nabla \phi_i)$$

is computed by

$$(\mathbf{I} - \mathbf{\Pi}^\nabla)^T (\mathbf{I} - \mathbf{\Pi}^\nabla).$$

Another choice of the stabilization term is the $H^{\frac{1}{2}}$-inner product [31],

$$\begin{aligned} S_{\mathcal{E}}^{K}(u_h, v_h) : &= \sum_{E \subset \partial K} (u_h, v_h)_{H^{1/2}(E)} \\ &= \sum_{E \subset \partial K} \int_E \int_E \frac{(u_h(\mathbf{x}) - u_h(\mathbf{y}))\,(v_h(\mathbf{x}) - v_h(\mathbf{y}))}{\|\mathbf{x} - \mathbf{y}\|^2}\, d\mathbf{x} d\mathbf{y} \\ &= \sum_{E \subset \partial K} \delta_E(u_h)\delta_E(v_h), \end{aligned} \tag{3.13}$$

where δ_E is the difference between the nodal function values at the two end points of E. The matrix corresponding to this stabilization term can be simply computed as

$$(\mathbf{I} - \mathbf{\Pi}^{\nabla})^T \mathbf{W} (\mathbf{I} - \mathbf{\Pi}^{\nabla}),$$

where $\mathbf{W}$ looks like a $N_V \times N_V$ tridiagonal matrix with the sequence of entries $(-1, 2, -1)$ and moreover $(\mathbf{W})_{1,N_V} = (\mathbf{W})_{N_V,1} = -1$. Hence, we note that the bilinear form $a_h^K(\cdot,\cdot)$ is computed by the degrees of freedom $V_1(K)$ for both cases.

3.3 Construction of the Right Hand Side

We use an approximation technique for the right hand side presented in [12]. Let f_0^K be a piecewise constant approximation of f. Then, we define

$$F_h(v_h) := \sum_{K \in \mathcal{K}_h} \int_K f_0^K \bar{v}_h \, d\mathbf{x} = \sum_{K \in \mathcal{K}_h} |K| f_0^K \bar{v}_h,$$

where

$$\bar{v}_h := \frac{1}{N_V} \sum_{i=1}^{N_V} v_h(\mathbf{x}_i).$$

Therefore, we obtain an approximation estimate (see [12] for details),

$$F_h(v_h) - F(v_h) \leq Ch \left(\sum_{K \in \mathcal{T}_h} |f|^2_{H^1(K)} \right)^{1/2} |v_h|_{H^1(\Omega)} . \tag{3.14}$$

Chapter 4

Edge-Averaged Virtual Element Scheme

The weak formulation (2.2) for the convection-diffusion problem (2.1) is to seek $u \in H_0^1(\Omega)$ such that

$$B(u,v) = \sum_{K\in\mathcal{K}_h} B^K(u,v) = F(v), \quad \forall v \in H_0^1(\Omega).$$

Then, since $V_1(\mathcal{K}_h) \subset H_0^1(\Omega)$, the bilinear form

$$B^K(u_h, v_h) = \int_K J(u_h)\cdot\nabla v_h \, d\mathbf{x} \tag{4.1}$$

is well-defined for $u_h, v_h \in V_1(\mathcal{K}_h)$. The main idea is to approximate the local flux $J(u_h)|_K$ in the local edge virtual element space $\mathbf{V}_0(K)$, and the approximation will be simply computed by some function values on edges or vertices.

4.1 A Flux Approximation in Virtual Element Spaces

We present a flux approximation for $J(u_h)$ in K using the degrees of freedom in $\mathbf{V}_0(K)$. From the lemma 3.1 in [49], we have for any $E \subset \partial K$,

$$\delta_E(e^{\psi_E} u) = \frac{1}{|E|} \int_E \kappa_E^{-1} (J(u) \cdot \boldsymbol{\tau}_E)\, ds, \tag{4.2}$$

for a given $u \in H_0^1(\Omega) \cap C^0(\bar{\Omega})$. This identity can easily be extended to any line segment linking two vertices of K. Then, the flux approximation $J_K \in \mathbf{V}_0(K)$ is obtained by the relation

$$\mathrm{dof}_E(\kappa_E^{-1} J_K) = \mathrm{dof}_E(\kappa_E^{-1} J(u_h)) = \delta_E(e^{\psi_E} u_h),$$

for all $E \subset \partial K$. Hence, the approximation $J_K \in \mathbf{V}_0(K)$ is written as

$$J(u_h)|_K \approx J_K = \sum_{E \subset \partial K} (J_K \cdot \boldsymbol{\tau}_E) \boldsymbol{\chi}_E,$$

where $\boldsymbol{\chi}_E$ is the canonical basis of $\mathbf{V}_0(K)$ on each edge E. For any $E \subset \partial K$, we have $J_K \cdot \boldsymbol{\tau}_E \in \mathcal{P}_0(E)$, which means that

$$J_K \cdot \boldsymbol{\tau}_E = \tilde{\kappa}_E \delta_E(e^{\psi_E} u_h), \tag{4.3}$$

where

$$\tilde{\kappa}_E = \left(\frac{1}{|E|} \int_E \kappa_E^{-1}\, ds \right)^{-1}.$$

From the identity (4.3), we conclude that each degree of freedom of $J_K \in \mathbf{V}_0(K)$ can be expressed by nodal values of $e^{\psi_E} u_h$ at the vertices of K. Thus, not only are the continuity or exact form of some functions inside K not imposed, but also the locally defined function

ψ_E in Remark 2.1 can be simply used. Moreover, it is clear to see that $J(u_h) = J_K$ if $J(u_h) \in \mathbf{V}_0(K)$.

An approximating bilinear form $\bar{B}_h^K(\cdot,\cdot)$

We present an approximating bilinear form with the flux approximation J_K. By substituting J_K for $J(u_h)$ in (4.1), we define a bilinear form

$$\bar{B}_h^K(u_h, v_h) = \sum_{E\subset\partial K} \tilde{\kappa}_E \delta_E(e^{\psi_E} u_h) \int_K \boldsymbol{\chi}_E \cdot \nabla v_h \, d\mathbf{x}. \tag{4.4}$$

Then, it follows from (4.2) and (4.3) that

$$\begin{aligned} \bar{B}_h^K(u_I, v_h) &= \sum_{E\subset\partial K} \tilde{\kappa}_E \delta_E(e^{\psi_E} u) \int_K \boldsymbol{\chi}_E \cdot \nabla v_h \, d\mathbf{x} \\ &= \sum_{E\subset\partial K} \left(\frac{\tilde{\kappa}_E}{|E|} \int_E \kappa_E^{-1} (J(u)\cdot\boldsymbol{\tau}_E) \, ds \right) \int_K \boldsymbol{\chi}_E \cdot \nabla v_h \, d\mathbf{x}, \end{aligned} \tag{4.5}$$

where u_I is the nodal interpolant in $V_1(\mathcal{K}_h)$ of any continuous function u over $\bar{\Omega}$ in $H_0^1(\Omega)$. We note that it is still difficult to handle the bilinear form (4.4) because the exact forms of $\boldsymbol{\chi}_E$ and v_h are needed for the integration over K. We could approximate the integration using the L^2-projection $\boldsymbol{\Pi}_0^0$ over $\mathbf{V}_0(K)$, but this approach does not explicitly show the relation between the bilinear form and the corresponding stiffness matrix. More importantly, a simple modification with the assumption that J_K is constant implies another approximating bilinear form. This bilinear form leads us to a stabilized virtual element scheme.

4.2 Derivation of the EAVE Bilinear Form

The key idea is to simplify the bilinear form $\bar{B}_h^K(u_h, v_h)$ under the assumption that J_K is a constant vector on K. Based on the simplified formula, a new approximating bilinear form $B_h^K(u_h, v_h)$ will be defined. The following lemma provides the details for the simplification.

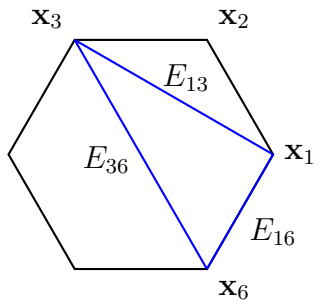

Figure 4.1: Examples of line segments linking two vertices in a polygon.

Lemma 4.1. *Let E_{ij} be a line segment linking two vertices $\mathbf{x}_i$ and $\mathbf{x}_j$ for $i < j$ (e.g. Figure 4.1). If J_K is a constant vector on K, then for any $v_h \in V_1(K)$,*

$$\sum_{E \subset \partial K} (J_K \cdot \boldsymbol{\tau}_E) \int_K \boldsymbol{\chi}_E \cdot \nabla v_h \, d\mathbf{x} = \sum_{1 \le i < j \le N_V} \omega_{ij}^K \tilde{\kappa}_{E_{ij}} \delta_{ij}^K (e^{\psi_{E_{ij}}} u_h) \delta_{ij}^K (v_h), \tag{4.6}$$

where $\omega_{ij}^K = -a_h^K(\phi_i, \phi_j)$, $\delta_{ij}^K(v_h) = v_h(\mathbf{x}_j) - v_h(\mathbf{x}_i)$, and $\tilde{\kappa}_{E_{ij}}$ is the harmonic average on E_{ij} for $1 \le i < j \le N_V$.

Proof. We assume that J_K is a constant vector on K. Then,

$$\Phi_K(\mathbf{x}) := J_K \cdot \mathbf{x}$$

is a linear polynomial for $\mathbf{x} \in K$. Let us simply write $\sigma_i = J_K \cdot \mathbf{x}_i$ for $1 \le i \le N_V$. Since $J_K \in \mathbf{V}_0(K)$ and $\Phi_K \in V_1(K)$, it follows from the unisolvent conditions of $\mathbf{V}_0(K)$ and $V_1(K)$

that

$$J_K = \sum_{E \subset \partial K} (J_K \cdot \boldsymbol{\tau}_E) \boldsymbol{\chi}_E \quad \text{and} \quad \Phi_K(\mathbf{x}) = \sum_{i=1}^{N_V} \sigma_i \phi_i(\mathbf{x})$$

in $\mathbf{V}_0(K)$ and $V_1(K)$, respectively. We also obtain

$$\begin{aligned} \int_K J_K \cdot \nabla v_h \, d\mathbf{x} &= \int_K \nabla \Phi_K \cdot \nabla v_h \, d\mathbf{x} \\ &= \int_K \nabla \Pi_1^\nabla \Phi_K \cdot \nabla \Pi_1^\nabla v_h \, d\mathbf{x} + S^K(\Phi_K - \Pi_1^\nabla \Phi_K, v_h - \Pi_1^\nabla v_h) \end{aligned}$$

because $\Phi_K = \Pi_1^\nabla \Phi_K$. We now focus on the first term

$$\int_K \nabla \Pi_1^\nabla \Phi_K \cdot \nabla \Pi_1^\nabla v_h \, d\mathbf{x} = \int_K \left(\sum_{i=1}^{N_V} \sigma_i \nabla \Pi_1^\nabla \phi_i \right) \cdot \left(\sum_{i=1}^{N_V} v_h(\mathbf{x}_i) \nabla \Pi_1^\nabla \phi_i \right) d\mathbf{x}. \tag{4.7}$$

We have seen that $\sum_{i=1}^{N_V} \nabla \phi_i \in \mathbf{V}_0(K)$, and all its degrees of freedom in $\mathbf{V}_0(K)$ are zero. Hence, $\sum_{i=1}^{N_V} \nabla \phi_i \equiv \mathbf{0}$ in $\mathbf{V}_0(K)$, and equivalently

$$\int_K \nabla \Pi_1^\nabla \phi_j \cdot \nabla \Pi_1^\nabla \phi_j \, d\mathbf{x} = - \sum_{i=1, i \neq j} \int_K \nabla \Pi_1^\nabla \phi_j \cdot \nabla \Pi_1^\nabla \phi_i \, d\mathbf{x}.$$

Using this fact, we distribute the integrant of the right hand side in (4.7) and factor out with respect to

$$\int_K \nabla \Pi_1^\nabla \phi_i \cdot \nabla \Pi_1^\nabla \phi_j \, d\mathbf{x}$$

for $i < j$. Then, each term becomes

$$\begin{aligned} &(\sigma_i v_h(\mathbf{x}_j) + \sigma_j v_h(\mathbf{x}_i) - \sigma_i v_h(\mathbf{x}_i) - \sigma_j v_h(\mathbf{x}_j)) \int_K \nabla \Pi_1^\nabla \phi_i \cdot \nabla \Pi_1^\nabla \phi_j \, d\mathbf{x} \\ &\quad = (v_h(\mathbf{x}_j) - v_h(\mathbf{x}_i))(\sigma_j - \sigma_i) \left(- \int_K \nabla \Pi_1^\nabla \phi_i \cdot \nabla \Pi_1^\nabla \phi_j \, d\mathbf{x} \right). \end{aligned}$$

In this case, the factor $\sigma_j - \sigma_i$ is written as

$$\sigma_j - \sigma_i = J_K \cdot \boldsymbol{\tau}_{ij} = \tilde{\kappa}_{E_{ij}} \delta_{ij}^K (e^{\psi_{E_{ij}}} u_h),$$

where $\boldsymbol{\tau}_{ij} = \mathbf{x}_j - \mathbf{x}_i$.

We treat the second term in a similar way. We already know that $\sum_{i=1}^{N_V} \phi_i \equiv 1$ in $V_1(K)$ from the unisolvent condition, which implies that

$$S^K(\phi_j - \Pi_1^\nabla \phi_j, \phi_j - \Pi_1^\nabla \phi_j) = - \sum_{i=1, i\neq j}^{N_V} S^K(\phi_j - \Pi_1^\nabla \phi_j, \phi_i - \Pi_1^\nabla \phi_i).$$

Likewise, if we distribute the second term and factor it out with respect to

$$S^K(\phi_j - \Pi_1^\nabla \phi_i, \phi_j - \Pi_1^\nabla \phi_j)$$

for $i < j$, then we complete to prove it. □

Consequently, we define the EAVE bilinear form on an element K as

$$B_h^K(u_h, v_h) = \sum_{1 \le i < j \le N_V} \omega_{ij}^K \tilde{\kappa}_{E_{ij}} \delta_{ij}^K (e^{\psi_{E_{ij}}} u_h) \delta_{ij}^K (v_h). \tag{4.8}$$

The discrete problem for the EAVE scheme is defined to find $u_h \in V_1(\mathcal{K}_h)$ such that

$$\sum_{K \in \mathcal{K}_h} B_h^K(u_h, v_h) = F_h(v_h), \quad \forall v_h \in V_1(\mathcal{K}_h). \tag{4.9}$$

Moreover, it follows from (4.2) that

$$B_h^K(u_I, v_h) = \sum_{1 \le i < j \le N_V} \omega_{ij}^K \left(\frac{\tilde{\kappa}_{E_{ij}}}{|\boldsymbol{\tau}_{ij}|} \int_{E_{ij}} \kappa_{E_{ij}}^{-1} (J(u) \cdot \boldsymbol{\tau}_{ij}) \, ds \right) \delta_{ij}^K (v_h). \tag{4.10}$$

Remark 4.1. *We emphasize that* ω_{ij}^K *are computable and already given in the virtual element methods for Poisson problems. In order to compute the bilinear form* (4.8)*, we need the nodal degrees of freedom* (3.1) *of* $u_h, v_h \in V_1(K)$ *and the locally defined function* $\psi_{E_{ij}}$ *on the line segment* E_{ij}*. More exactly, the local function can be given as* $\psi_{E_{ij}}(\mathbf{x}) = {\alpha_{E_{ij}}}^{-1}\boldsymbol{\beta}_{E_{ij}} \cdot \mathbf{x}$ *with constant approximations* $\alpha_{E_{ij}}$ *and* $\boldsymbol{\beta}_{E_{ij}}$ *on* E_{ij}*. Therefore, the bilinear form is computed by*

$$\tilde{\kappa}_{E_{ij}}\delta_{E_{ij}}^K(e^{\psi_{E_{ij}}}u_h) = \alpha_{E_{ij}}\mathbb{B}(\alpha_{E_{ij}}{}^{-1}\boldsymbol{\beta}_{E_{ij}} \cdot (\mathbf{x}_i - \mathbf{x}_j))u_j - \alpha_{E_{ij}}\mathbb{B}(\alpha_{E_{ij}}{}^{-1}\boldsymbol{\beta}_{E_{ij}} \cdot (\mathbf{x}_j - \mathbf{x}_i))u_i,$$

where $\mathbb{B}(z)$ *is the Bernoulli function defined in* (2.13)*.*

In summary, we approximate the local bilinear form (4.1) using the flux approximation in the local edge virtual element space $\mathbf{V}_0(K)$, and then approximate the form (4.4) under the assumption that J_K is a constant vector in K,

$$B^K(u_h, v_h) \approx \bar{B}_h^K(u_h, v_h) \approx B_h^K(u_h, v_h).$$

We note that these approximate relations become equalities if $J(u_h)$ is a constant vector on K. The assumption that $J(u_h)$ is constant will be a key condition in error analysis.

4.3 Monotonicity

The following lemma shows that the EAVE method is monotone if the stiffness matrix from $a_h^K(\phi_i, \phi_j)$ is an M-matrix.

Lemma 4.2. *If the stiffness matrix for the Poisson equation with the virtual bilinear form* (3.10) *is an M-matrix, then the stiffness matrix from the EAVE method* (4.9) *is an M-matrix for* $\alpha \in C^0(\bar{\Omega})$ *and* $\boldsymbol{\beta} \in \left(C^0(\bar{\Omega})\right)^2$*.*

Proof. We consider the stiffness matrix whose components are

$$B_{mn} = \sum_{K \in \mathcal{K}_h} B_h^K(\phi_n, \phi_m).$$

If $m \neq n$, it is clear to see that $B_{mn} = 0$ if the two corresponding vertices to ϕ_m and ϕ_n do not share a polygon in $\mathcal{K}_h$. Otherwise, we let $\mathcal{K}_{mn}$ be the set of polygons shared by the two vertices $\mathbf{x}_m$ and $\mathbf{x}_n$. Then, each component becomes

$$B_{mn} = \sum_{K \in \mathcal{K}_{mn}} B_h^K(\phi_n, \phi_m).$$

For any polygon $K \in \mathcal{K}_{mn}$, we have

$$B_h^K(\phi_n, \phi_m) = -\omega_{mn}^K \tilde{\kappa}_{E_{mn}} e^{\psi_{E_{mn}}(\mathbf{x}_n)} \quad \text{or} \quad -\omega_{nm}^K \tilde{\kappa}_{E_{nm}} e^{\psi_{E_{nm}}(\mathbf{x}_n)}.$$

Note that $B_h^K(\phi_n, \phi_m)$ depends on the local indices of m and n which are determined counterclockwise in K. Hence, since $\omega_{mn}^K = -a_h^K(\phi_m, \phi_n) \geq 0$ and $\tilde{\kappa}_{E_{mn}} > 0$, it is easy to see that $B_{mn} \leq 0$.

Moreover, it follows from the unisolvent condition in $V_1(K)$ that

$$\sum_m B_{mn} = \sum_{K \in \mathcal{K}_h} B_h^K(\phi_n, 1) = 0.$$

if $\mathbf{x}_n$ has no neighbor on the boundary. If $\mathbf{x}_n$ has a neighbor on the boundary, then $\sum_m B_{mn} > 0$.

□

Chapter 5

Error Analysis

In this chapter, we will prove the discrete inf-sup condition to guarantee the solvability of the discrete problem (4.9). This inf-sup condition will be also used to show the order of convergence in terms of

$$h := \max_{K \in \mathcal{K}_h} h_K,$$

where h_K is the diameter of each element $K \in \mathcal{K}_h$.

5.1 Some Estimates of the Bilinear Forms

In this section, we show upper bounds of the difference between the bilinear forms $B^K(\cdot,\cdot)$ and $B_h^K(\cdot,\cdot)$. These bounds will be used to prove the discrete inf-sup condition. The key condition is that

$$B^K(w, v_h) = \bar{B}_h^K(w, v_h) = B_h^K(w, v_h), \quad \forall v_h \in V_1(K)$$

if $J(w)$ is a constant vector.

The norm equivalence between L^p-norm and L^2-norm in the finite dimensional space $V_1(K)$ will be used. It is well known that all norms in finite dimensional vector spaces are equivalent. However, since all types of shape-regular polygons are considered, it is not clear to show how the constant involved in the norm equivalence depends on the properties of polygons. The constant may not bounded in some cases. Hence, for a finite dimensional vector space $\mathbb{V}_h(K)$, we define

$$C(K) := \sup_{\mu \in \mathbb{V}_h(K)} \frac{\|\mu\|_{L^p(K)}}{\|\mu\|_{L^2(K)}}$$

with $h_K = 1$, and we prove that $C(K)$ is uniformly bounded for any shape-regular polygon K.

Lemma 5.1. *(Norm Equivalence) Let $\mathbb{V}_h(K)$ be a finite dimensional subspace of $L^p(K)$ for any $p > 1$. Then, every element $\mu \in \mathbb{V}_h(K)$ satisfies*

$$\|\mu\|_{L^p(K)} \leq C h_K^{2/p-1} \|\mu\|_{L^2(K)}, \tag{5.1}$$

where C is a generic constant independent of h_K.

Proof. See Appendix A. □

We present and prove the following result.

Lemma 5.2. *Let p, q, r, and η have the relations,*

$$\frac{1}{p} + \frac{1}{q} = 1 \quad \textit{and} \quad \frac{1}{q} = \frac{1}{r} - \frac{\eta}{2}$$

with $0 < \eta < 1$ and $1 \leq r < 2$. For any $K \in \mathcal{K}_h$, we assume that $w \in C(\bar{\Omega})$ and

$J(w) \in (W^{\eta,r}(K))^2$. *Then, for any* $v_h \in V_1(K)$, *it holds that*

$$\left|B^K(w, v_h) - B_h^K(w_I, v_h)\right| \leq C h_K^{1/p-1/q} \left|J(w)\right|_{W^{\eta,r}(K)} \left|v_h\right|_{H^1(K)}.$$

Proof. From (4.5) and (4.10), the difference is written as

$$B^K(w, v_h) - B_h^K(w_I, v_h) = \mathcal{E}_1(J(w), v_h) + \mathcal{E}_2(J(w), v_h),$$

where $\mathcal{E}_1(J(w), v_h) = B^K(w, v_h) - \bar{B}_h^K(w_I, v_h)$ and $\mathcal{E}_2(J(w), v_h) = \bar{B}_h^K(w_I, v_h) - B_h^K(w_I, v_h)$. In this case, $\mathcal{E}_i(\cdot, v_h)$ for $i = 1, 2$ are considered as linear functionals, so we first show that they are continuous (or bounded) linear functionals. With scaled elements $\hat{K} := \{\hat{\mathbf{x}} \mid \hat{\mathbf{x}} = \mathbf{x}/h_K, \mathbf{x} \in K\}$ and scaled functions $\widehat{v_h}(\hat{\mathbf{x}}) := v_h(h_K\hat{\mathbf{x}}) = v_h(\mathbf{x})$, it follows from the change of variables that

$$B^K(w, v_h) = \int_K J(w) \cdot \nabla v_h \, d\mathbf{x} = h_K \int_{\hat{K}} \widehat{J(w)} \cdot \hat{\nabla} \widehat{v_h} \, d\hat{\mathbf{x}}.$$

Then, the scaled integration is bounded as

$$\left| \int_{\hat{K}} \widehat{J(w)} \cdot \hat{\nabla} \widehat{v_h} \, d\hat{\mathbf{x}} \right| \leq \|\widehat{J(w)}\|_{L^q(\hat{K})} \left|\widehat{v_h}\right|_{W^{1,p}(\hat{K})} \tag{5.2}$$

using Hölder's inequality with $1/p + 1/q = 1$. It also follows from (4.5), (4.10), and the same scaling that

$$\left|h_K^{-1} \bar{B}_h^K(w_I, v_h)\right| \leq C \|\widehat{J(w)}\|_{L^q(\hat{K})} \left|\widehat{v_h}\right|_{W^{1,p}(\hat{K})}, \tag{5.3}$$

and

$$\left|h_K^{-1} B_h^K(w_I, v_h)\right| \leq C \|\widehat{J(w)}\|_{L^q(\hat{K})} \left|\widehat{v_h}\right|_{W^{1,p}(\hat{K})}. \tag{5.4}$$

Let us denote the scaled functionals as

$$\widehat{\mathcal{E}}_i(\widehat{J(w)}, \widehat{v_h}) := \frac{1}{h_K}\mathcal{E}_i(J(w), v_h), \quad i = 1, 2.$$

From (5.2), (5.3), (5.4), and the Sobolev embedding theorem [1], we have

$$\begin{aligned}\widehat{\mathcal{E}}_i(\widehat{J(w)}, \widehat{v_h}) &\le C_i \|\widehat{J(w)}\|_{L^q(\hat{K})} \, |\widehat{v_h}|_{W^{1,p}(\hat{K})} \\ &\le C_i \|\widehat{J(w)}\|_{W^{\eta,r}(\hat{K})} \, |\widehat{v_h}|_{W^{1,p}(\hat{K})} \,,\end{aligned}$$

for $0 < \eta < 1$ and $1 \le r < 2$. The constants C_i may vary at each line. Hence, the scaled linear functionals $\widehat{\mathcal{E}}_i(\cdot, \widehat{v_h})$ are bounded above. From (4.5), (4.10), and Lemma 4.1, we have $\widehat{\mathcal{E}}_i(\widehat{J(w)}, \widehat{v_h}) = 0$ if $J(w)$ is a constant on K. Therefore, it follows from Theorem 6.1 in [35] and the Blamble-Hilbert lemma that

$$\begin{aligned}h_K^{-1}\mathcal{E}_i(J(w), v_h) &= \widehat{\mathcal{E}}_i(\widehat{J(w)}, \widehat{v_h}) \\ &\le C_i |\widehat{J(w)}|_{W^{\eta,r}(\hat{K})} \, |\widehat{v_h}|_{W^{1,p}(\hat{K})} \,.\end{aligned}$$

By scaling back to K and using Lemma 5.1, we get

$$\mathcal{E}_i(J(w), v_h) \le C h_K^{1/p-1/q} |J(w)|_{W^{\eta,r}(K)} \, |v_h|_{H^1(K)} \,.$$

□

Similarly, another upper bound is given with different norms.

Lemma 5.3. *If we assume that $w \in C(\bar{\Omega})$ and $J(w) \in (W^{1,s}(K))^2$ with $s > 2$ for any $K \in \mathcal{K}_h$, then*

$$\left|B^K(w, v_h) - B_h^K(w_I, v_h)\right| \le C h_K^{2-2/s} \, |J(w)|_{W^{1,s}(K)} \, |v_h|_{H^1(K)} \,,$$

for any $v_h \in V_1(\mathcal{K}_h)$.

Proof. The proof of this lemma is similar to that of the previous lemma. We look at the same expression

$$B^K(w, v_h) - B_h^K(w_I, v_h) = \mathcal{E}_1(J(w), v_h) + \mathcal{E}_2(J(w), v_h),$$

and we bound the scaled linear functionals $\widehat{\mathcal{E}}_i(\cdot, \widehat{v_h})$ in different norms. Indeed, we obtain an upper bound

$$\left| \int_{\hat{K}} \widehat{J(w)} \cdot \hat{\nabla} \widehat{v_h} \, d\hat{\mathbf{x}} \right| \leq C_{\hat{K}} \|\widehat{J(w)}\|_{L^\infty(\hat{K})} \, |\widehat{v_h}|_{H^1(\hat{K})} \, .$$

By applying the same scaling to the intermediate term (4.5), we have

$$\bar{B}_h^K(w_I, v_h) = h_K \sum_{\hat{E} \subset \partial \hat{K}} \left(\frac{\tilde{\hat{\kappa}}_{\hat{E}}}{|\boldsymbol{\tau}_{\hat{E}}|} \int_{\hat{E}} \hat{\kappa}_{\hat{E}}^{-1} (\widehat{J(w)} \cdot \boldsymbol{\tau}_{\hat{E}}) \, d\hat{s} \right) \int_{\hat{K}} \boldsymbol{\chi}_{\hat{E}} \cdot \hat{\nabla} \widehat{v_h} \, d\hat{\mathbf{x}},$$

where

$$\tilde{\hat{\kappa}}_{\hat{E}} = \left(\frac{1}{|\boldsymbol{\tau}_{\hat{E}}|} \int_{\hat{E}} \hat{\kappa}_{\hat{E}}^{-1} \, d\hat{s} \right)^{-1} .$$

Thus, we have an upper bound for the scaled version of (4.5),

$$\left| h_K^{-1} \bar{B}_h^K(w_I, v_h) \right| \leq C_{\alpha,\boldsymbol{\beta}} \|\widehat{J(w)}\|_{L^\infty(\hat{K})} \, |\widehat{v_h}|_{H^1(\hat{K})} \, .$$

The constant $C_{\alpha,\boldsymbol{\beta}}$ may depend on $\|\boldsymbol{\chi}_{\hat{E}}\|_{L^2(\hat{K})}$, which is guaranteed to be properly bounded because $\boldsymbol{\chi}_{\hat{E}}$ is a basis for a finite-dimensional space $\mathbf{V}_0(K)$. For (4.10), it follows from the same scaling that

$$B_h^K(w_I, v_h) = h_K \sum_{1 \leq i < j \leq N_V} \omega_{ij}^{\hat{K}} \left(\frac{\tilde{\hat{\kappa}}_{\hat{E}_{ij}}}{|\boldsymbol{\tau}_{ij}|} \int_{\hat{E}_{ij}} \hat{\kappa}_{\hat{E}_{ij}}^{-1} (\widehat{J(w)} \cdot \boldsymbol{\tau}_{ij}) \, d\hat{s} \right) \delta_{ij}^{\hat{K}}(\widehat{v_h}),$$

where i and j are the indices of the vertices of $\hat{K}$ that coincide with those of K. Since we have a bound of $\omega_{ij}^{\hat{K}}$ from (3.11),

$$|\omega_{ij}^{\hat{K}}| \leq \gamma^* |\phi_i|_{H^1(\hat{K})} |\phi_j|_{H^1(\hat{K})},$$

the scaled one for (4.10) is bounded as

$$\left| h_K^{-1} B_h^K(w_I, v_h) \right| \leq C_{\alpha,\boldsymbol{\beta}} \|\widehat{J(w)}\|_{L^\infty(\hat{K})} \, |\widehat{v_h}|_{H^1(\hat{K})} \, .$$

The constant $C_{\alpha,\boldsymbol{\beta}}$ in this case may contain $|\phi_i|_{H^1(\hat{K})}$, but it is bounded by a constant so that it is omitted. Thus, the scaled linear functionals $\widehat{\mathcal{E}}_i(\cdot, \widehat{v_h})$ are bounded with respect to L^∞-norm and H^1-seminorm. By the Sobolev embedding theorem [1] and the Blamble-Hilbert lemma, we get

$$\begin{aligned}
\widehat{\mathcal{E}}_i(\widehat{J(w)}, \widehat{v_h}) &\leq C \|\widehat{J(w)}\|_{L^\infty(\hat{K})} \, |\widehat{v_h}|_{H^1(\hat{K})} \\
&\leq C \|\widehat{J(w)}\|_{W^{1,s}(\hat{K})} \, |\widehat{v_h}|_{H^1(\hat{K})} \\
&\leq C |\widehat{J(w)}|_{W^{1,s}(\hat{K})} \, |\widehat{v_h}|_{H^1(\hat{K})} \\
&= C h_K^{1-2/s} |J(w)|_{W^{1,s}(K)} \, |v_h|_{H^1(K)} \, ,
\end{aligned}$$

for $s > 2$.

□

From the Lemma 5.2, we will derive another upper bound for the difference $B^K(w_h, v_h) - B_h^K(w_h, v_h)$ with respect to $|w_h|_{H^1(K)}$ and $|v_h|_{H^1(K)}$. In this case, it is important to know that $|w_h|_{H^2(K)} \neq 0$ for the virtual element function $w_h \in V_1(K)$ while $|p_1|_{H^2(T)} = 0$ for $p_1 \in \mathcal{P}_1(\mathcal{T}_h)$ in the standard linear finite element method. Instead, we use the regularity result presented in [9, 34, 40] that there exists $\eta \in (0, 1)$ such that $|w_h|_{H^{1+\eta}(K)} = 0$.

Lemma 5.4. *For any $K \in \mathcal{K}_h$, we assume that $J(w_h) \in (W^{\eta,r}(K))^2$ for any $w_h \in V_1(K)$. Then, we have*

$$\left|B^K(w_h, v_h) - B_h^K(w_h, v_h)\right| \leq C_{\boldsymbol{\beta}} h_K \left|w_h\right|_{H^1(K)} \left|v_h\right|_{H^1(K)},$$

where the constant $C_{\boldsymbol{\beta}}$ is independent of h_K.

Proof. From Lemma 5.2, we have

$$\left|B^K(w_h, v_h) - B_h^K(w_h, v_h)\right| \leq C h_K^{1/p-1/q} |J(w_h)|_{W^{\eta,r}(K)} \left|v_h\right|_{H^1(K)}$$

for all $w_h, v_h \in V_1(K)$. For any given polygon K, the constant $\eta \in (0,1)$ is chosen to satisfy

$$|w_h|_{H^{1+\eta}(K)} \leq C \|\Delta w_h\|_{H^{-1+\eta}(K)} = 0$$

(see e.g., [9, 34, 40]). Hence, Lemma 5.1 provides the following estimate

$$|J(w_h)|_{W^{\eta,r}(K)} \leq C h_K^{2/r-1} |J(w_h)|_{H^\eta(K)},$$

and Proposition 2.2 in [45] implies that

$$\begin{aligned} |J(w_h)|_{H^\eta(K)} &\leq |\alpha \nabla w_h + \boldsymbol{\beta} w_h|_{H^\eta(K)} \\ &\leq |\alpha|_{H^\eta(K)} \left|w_h\right|_{H^{1+\eta}(K)} + |\boldsymbol{\beta}|_{H^\eta(K)} \left|w_h\right|_{H^\eta(K)} \\ &\leq h_K^{1-\eta} \left|\boldsymbol{\beta}\right|_{H^\eta(K)} \left|w_h\right|_{H^1(K)}. \end{aligned}$$

Therefore, it follows from the relations in Lemma 5.2 that

$$\frac{1}{p} - \frac{1}{q} + \frac{2}{r} - 1 + 1 - \eta = 1,$$

and one can see that the constant $C_{\boldsymbol{\beta}}$ contains $|\boldsymbol{\beta}|_{H^{\eta}(K)}$.

□

5.2 Well-Posedness of the Discrete Problem

Basically, our strategy to prove the discrete inf-sup condition is to observe that for $w_h, v_h \in V_1(\mathcal{K}_h)$,

$$B_h(w_h, v_h) \geq B(w_h, v_h) - |B_h(w_h, v_h) - B(w_h, v_h)| .$$

Then, the difference between the two bilinear forms can be controlled by Lemma 5.4, and the first term is done by the following inf-sup condition: For a constant $C_B > 0$, it holds

$$\sup_{v_h \in V_1(\mathcal{K}_h)} \frac{B(w_h, v_h)}{\|v_h\|_{H^1(\Omega)}} \geq C_B \|w_h\|_{H^1(\Omega)}, \quad \forall w_h \in V_1(\mathcal{K}_h). \tag{5.5}$$

From (2.3), it is immediate to have the inf-sup condition in the space $H_0^1(\Omega)$, that is, there exists $v \in H_0^1(\Omega)$ such that

$$B(w, v) \geq \bar{C}_B \|w\|_{H^1(\Omega)} \|v\|_{H^1(\Omega)}, \quad \forall w \in H_0^1(\Omega),$$

for some constant $\bar{C}_B > 0$. Likewise, since $V_1(\mathcal{K}_h) \subset H_0^1(\Omega)$, there exists $v^* \in H_0^1(\Omega)$ such that

$$B(w_h, v^*) \geq \bar{C}_B \|w_h\|_{H^1(\Omega)} \|v^*\|_{H^1(\Omega)}, \quad \forall w_h \in V_1(\mathcal{K}_h).$$

However, this result is not enough to imply (5.5) because we cannot guarantee that $v^* \in V_1(\mathcal{K}_h)$. In this situation, we use the mathematical techniques in [16] to seek $v_h^* \in V_1(\mathcal{K}_h)$

satisfying the inequality for every $w_h \in V_1(\mathcal{K}_h)$. The proof is similar to that of [16], but we want to present it here because we consider a slightly different bilinear form,

$$a(w, v) = \int_\Omega \alpha(\mathbf{x}) \nabla w \cdot \nabla v \, d\mathbf{x},$$

for any $w, v \in H_0^1(\Omega)$.

Lemma 5.5. *Assume that* $0 < \alpha_{\min} \leq \alpha(\mathbf{x}) \leq \alpha_{\max}$. *For any given* $v^* \in H_0^1(\Omega)$, *there exists* $v_h^* \in V_1(\mathcal{K}_h)$ *such that*

$$a(v_h^*, v_h) = a(v^*, v_h), \quad \forall v_h \in V_1(\mathcal{K}_h). \tag{5.6}$$

Moreover, the error bounds are given as

$$\|v^* - v_h^*\|_{L^2(\Omega)} + h\|v^* - v_h^*\|_{H^1(\Omega)} \leq C_\alpha h \|v^*\|_{H^1(\Omega)}, \tag{5.7}$$

for some constant $C_\alpha > 0$ *depends on* α *but is independent of* h. *More precisely, the constant is presented as*

$$C_\alpha = C\alpha_{\max}\left(1 + \frac{\alpha_{\max}}{\alpha_{\min}}\right).$$

Proof. It is immediate to see that for any $v_h \in V_1(\mathcal{K}_h)$,

$$a(v_h, v_h) \geq \alpha_{\min} |v_h|^2_{H^1(\Omega)},$$

so the problem (5.6) has a unique solution. Moreover, we have

$$\alpha_{\min}\|v_h^*\|^2_{H^1(\Omega)} \leq a(v_h^*, v_h^*) = a(v^*, v_h^*) \leq \alpha_{\max}\|v^*\|_{H^1(\Omega)}\|v_h^*\|_{H^1(\Omega)},$$

which means that

$$\|v_h^*\|_{H^1(\Omega)} \leq \frac{\alpha_{\max}}{\alpha_{\min}} \|v^*\|_{H^1(\Omega)}. \tag{5.8}$$

In order to use the duality argument, we assume that $\varphi \in H^2(\Omega) \cap H_0^1(\Omega)$ is the solution of the variational problem,

$$a(\varphi, v) = (v^* - v_h^*, v)_{L^2(\Omega)}, \quad \forall v \in H_0^1(\Omega). \tag{5.9}$$

Since φ is a continuous function, its interpolant on $V_1(\mathcal{K}_h)$ is well-defined and denoted as φ_I. Then, by Proposition 4.3 in [12] and the regularity theorem, the interpolation error is bounded as

$$\|\varphi - \varphi_I\|_{H^1(\Omega)} \leq Ch\|\varphi\|_{H^2(\Omega)} \leq Ch\|v^* - v_h^*\|_{L^2(\Omega)}. \tag{5.10}$$

By choosing $v = v^* - v_h^*$ in (5.9) and applying (5.6), we have

$$\begin{aligned} \|v^* - v_h^*\|_{L^2(\Omega)}^2 &= a(\varphi, v^* - v_h^*) \\ &= a(\varphi - \varphi_I, v^* - v_h^*) + a(\varphi_I, v^* - v_h^*) \\ &= a(\varphi - \varphi_I, v^* - v_h^*). \end{aligned}$$

The Cauchy-Schwarz inequality and (5.10) imply that

$$\begin{aligned} a(\varphi - \varphi_I, v^* - v_h^*) &\leq \alpha_{\max} \|\varphi - \varphi_I\|_{H^1(\Omega)} \|v^* - v_h^*\|_{H^1(\Omega)} \\ &\leq C\alpha_{\max} h \|v^* - v_h^*\|_{L^2(\Omega)} \|v^* - v_h^*\|_{H^1(\Omega)}. \end{aligned}$$

Therefore, it follows from the triangle inequality and (5.8) that

$$\|v^* - v_h^*\|_{H^1(\Omega)} \leq \left(1 + \frac{\alpha_{\max}}{\alpha_{\min}}\right) \|v^*\|_{H^1(\Omega)},$$

which yields that

$$\|v^* - v_h^*\|_{L^2(\Omega)} \leq C_\alpha h \|v^*\|_{H^1(\Omega)}.$$

□

With the results in the above lemma, we prove the inf-sup condition (5.5) in the discrete space $V_1(\mathcal{K}_h)$ with a sufficiently small h. Similar mathematical techniques are also presented in [16].

Lemma 5.6. *(Inf-sup condition for $B(w_h, v_h)$) Assume that $0 < \alpha_{\min} \leq \alpha(\mathbf{x}) \leq \alpha_{\max}$, and $\boldsymbol{\beta} \in (W^{1,\infty}(K))^2$ for any $K \in \mathcal{K}_h$. Then, for a sufficiently small h satisfying*

$$h < h_0 = \bar{C}_B \left[C_\alpha \|\boldsymbol{\beta}\|_{W^{1,\infty}(\Omega)}\right]^{-1},$$

we have

$$\sup_{v_h \in V_1(\mathcal{K}_h)} \frac{B(w_h, v_h)}{\|v_h\|_{H^1(\Omega)}} \geq C_B \|w_h\|_{H^1(\Omega)}, \quad \forall w_h \in V_1(\mathcal{K}_h),$$

where

$$C_B = \frac{\alpha_{\min}}{\alpha_{\max}} \left(\bar{C}_B - C_\alpha \|\boldsymbol{\beta}\|_{W^{1,\infty}(\Omega)} h\right).$$

Proof. As we mentioned earlier, there exists $v^* \in H_0^1(\Omega)$ such that

$$B(w_h, v^*) \geq \bar{C}_B \|w_h\|_{H^1(\Omega)} \|v^*\|_{H^1(\Omega)}, \quad \forall w_h \in V_1(\mathcal{K}_h),$$

for some constant $\bar{C}_B > 0$. Let us denote

$$b(w, v) = \int_\Omega w\boldsymbol{\beta} \cdot \nabla v \, d\mathbf{x}.$$

Thus, it follows from (5.6) that there exists $v_h^* \in V_1(\mathcal{K}_h)$ such that

$$\begin{aligned} B(w_h, v_h^*) &= a(w_h, v_h^*) + b(w_h, v_h^*) \\ &= a(w_h, v^*) + b(w_h, v_h^* - v^*) + b(w_h, v^*) \\ &= B(w, v^*) + b(w_h, v_h^* - v^*). \end{aligned}$$

By applying the integration by parts and using the estimates (5.7), we obtain

$$\begin{aligned} b(w_h, v_h^* - v^*) &= \int_\Omega w_h\boldsymbol{\beta} \cdot \nabla(v_h^* - v^*) \, d\mathbf{x} \\ &= \int_\Omega \operatorname{div}(w_h\boldsymbol{\beta})(v_h^* - v^*) \, d\mathbf{x} \\ &\leq \|\operatorname{div}(w_h\boldsymbol{\beta})\|_{L^2(\Omega)} \|v_h^* - v^*\|_{L^2(\Omega)} \\ &\leq C_\alpha \|\boldsymbol{\beta}\|_{W^{1,\infty}(\Omega)} h \|w_h\|_{H^1(\Omega)} \|v^*\|_{H^1(\Omega)}. \end{aligned}$$

Therefore, we have a lower bound

$$B(w_h, v_h^*) \geq \bar{C}_B \|w_h\|_{H^1(\Omega)} \|v^*\|_{H^1(\Omega)} - C_\alpha \|\boldsymbol{\beta}\|_{W^{1,\infty}(\Omega)} h \|w_h\|_{H^1(\Omega)} \|v^*\|_{H^1(\Omega)}.$$

For any sufficiently small h satisfying

$$h < h_0 = \bar{C}_B \left[C_\alpha \|\boldsymbol{\beta}\|_{W^{1,\infty}(\Omega)} \right]^{-1},$$

we obtain from (5.8)

$$B(w_h, v_h^*) \geq C_B \|w_h\|_{H^1(\Omega)} \|v_h^*\|_{H^1(\Omega)},$$

where the constant $C_B > 0$ is expressed as

$$C_B = \frac{\alpha_{\min}}{\alpha_{\max}} \left(\bar{C}_B - C_\alpha \|\boldsymbol{\beta}\|_{W^{1,\infty}(\Omega)} h \right).$$

□

Therefore, our approximating bilinear form (4.8) satisfies the discrete inf-sup condition with a sufficiently small h. See also [42, 49] to find similar arguments in the standard linear finite element space.

Theorem 5.1. *Assume that $\alpha \in W^{1,\infty}(K)$, $\boldsymbol{\beta} \in (W^{1,\infty}(K))^2$, and $J(w_h) \in (W^{\eta,r}(K))^2$ for any $K \in \mathcal{K}_h$. Then, for a sufficiently small h satisfying*

$$h < \min\{h_0, h_1\} \quad \textit{where} \quad h_1 := C_B C_{\boldsymbol{\beta}}^{-1},$$

we have

$$\sup_{v_h \in V_1(\mathcal{K}_h)} \frac{B_h(w_h, v_h)}{\|v_h\|_{H^1(\Omega)}} \geq C_{B_h} \|w_h\|_{H^1(\Omega)}, \quad \forall w_h \in V_1(\mathcal{K}_h), \tag{5.11}$$

where $C_{B_h} = C_B - C_{\boldsymbol{\beta}} h$.

Proof. By Lemma 5.6, there exists $v_h \in V_1(\mathcal{K}_h)$ such that

$$\frac{B(w_h, v_h)}{\|v_h\|_{H^1(\Omega)}} \geq C_B \|w_h\|_{H^1(\Omega)}, \quad \forall w_h \in V_1(\mathcal{K}_h).$$

With the given function v_h, we observe the following identity

$$\frac{B_h(w_h, v_h)}{\|v_h\|_{H^1(\Omega)}} = \frac{B(w_h, v_h)}{\|v_h\|_{H^1(\Omega)}} + \frac{B_h(w_h, v_h) - B(w_h, v_h)}{\|v_h\|_{H^1(\Omega)}}.$$

We can see that the first term is easily bounded below, so we focus on the second one. Then,

it follows from Lemma 5.4 that

$$|B_h(w_h, v_h) - B(w_h, v_h)| \leq C_{\boldsymbol{\beta}} h \, \|w_h\|_{H^1(\Omega)} \, \|v_h\|_{H^1(\Omega)} .$$

Therefore, for any sufficiently small h satisfying

$$h < h_1 := C_B C_{\boldsymbol{\beta}}^{-1},$$

we have the following estimate

$$\frac{B_h(w_h, v_h)}{\|v_h\|_{H^1(\Omega)}} \geq C_{B_h} \|w_h\|_{H^1(\Omega)},$$

where $C_{B_h} = C_B - C_{\boldsymbol{\beta}} h$. □

5.3 Convergence Analysis

Finally, we obtain the convergence error estimate from Lemma 5.3.

Theorem 5.2. *Assume that* $\alpha \in W^{1,\infty}(K)$, $\boldsymbol{\beta} \in (W^{1,\infty}(K))^2$, *and* $J(w) \in (W^{1,s}(K))^2$ *for any* $K \in \mathcal{K}_h$. *Then, for* $h < \min\{h_0, h_1\}$, *we have*

$$\|u_I - u_h\|_{H^1(\Omega)} \leq Ch \left(\sum_{K \in \mathcal{K}_h} |J(u)|^2_{W^{1,s}(K)} + \sum_{K \in \mathcal{K}_h} |f|^2_{H^1(K)} \right)^{1/2} .$$

Proof. By choosing $w_h = u_I - u_h$, we have

$$\begin{aligned} C_{B_h}\|u_I - u_h\|_{H^1(\Omega)}\|v_h\|_{H^1(\Omega)} &\leq B_h(u_I - u_h, v_h) \\ &\leq B_h(u_I, v_h) - F_h(v_h) \\ &\leq B_h(u_I, v_h) - B(u, v_h) + F(v_h) - F_h(v_h) \end{aligned}$$

□

Chapter 6

Numerical Experiments

In this chapter, we conduct numerical experiments to check our theoretical results presented in the previous chapters. Several diffusion-dominated problems will be tested to check the convergence result. The stabilization effect of edge-averaged schemes will be shown by some convection-dominated problems. Numerical experiments are implemented by authors' codes developed based on iFEM [32].

The following mesh types on the square domains are considered:

- `para`: a mesh composed by structured parallelograms and triangles;
- `rand`: a Voronoi tessellation;
- `voro`: a Voronoi tessellation where the cell shapes are optimized via a Lloyd algorithm [48];
- `ncvx`: a mesh composed by structured non-convex polygons and triangles.

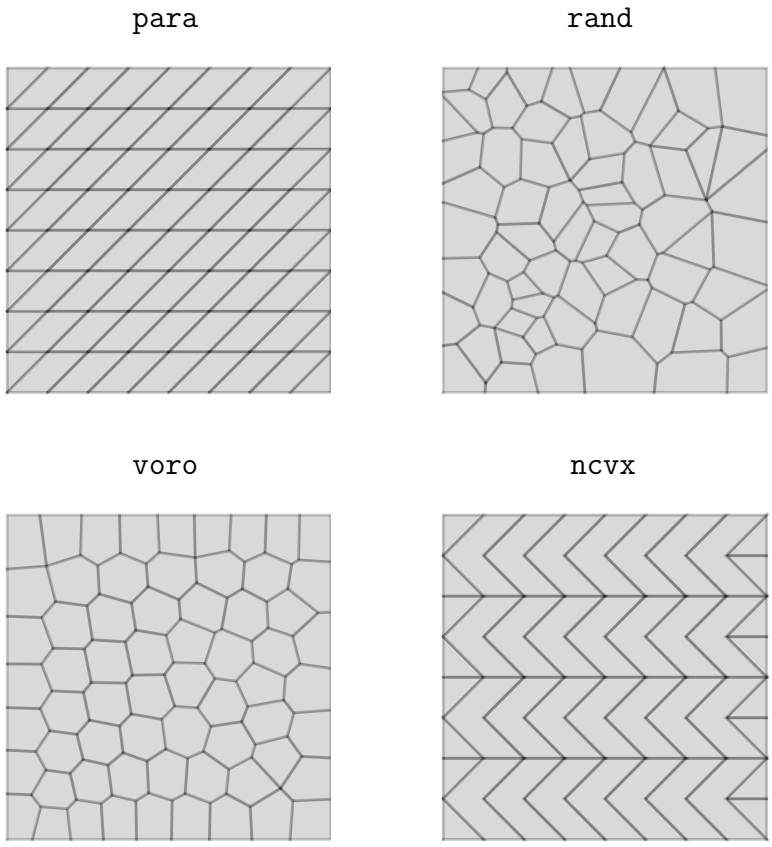

Figure 6.1: The mesh types on the square domain.

Since we do not have the exact form of v_h, we use some computable mesh-dependent norms. Using the bilinear form of the VEM for the Poisson equation, we define the A-norm as

$$\|v_h\|_A := \left(\sum_{K \in \mathcal{K}_h} a_h^K(v_h, v_h) \right)^{1/2}, \quad \forall v_h \in V_1(\mathcal{K}_h).$$

From the property of the bilinear form (3.11), the A-norm is equivalent to H^1-seminorm $|v_h|_{H^1(\Omega)}$. Another mesh-dependent L^∞-norm,

$$\|v_h\|_\infty := \max_i \left(\mathrm{dof}_i(|v_h|) \right), \quad \forall v_h \in V_1(\mathcal{K}_h),$$

is used to check existence of extreme spurious oscillations.

6.1 Diffusion-Dominated Problems

We numerically solve convection-diffusion problems in the diffusion-dominated regime using the EAVE method, and check the rate of convergence in the mesh-dependent norm errors.

Test problem 1: Diffusion-dominated

We consider the convection-diffusion problem [36] defined as

$$\begin{aligned} -\nabla \cdot (\alpha \nabla u + \boldsymbol{\beta} u) &= f \quad \text{in } \Omega = (-1,1) \times (-1,1), \\ u &= g \quad \text{on } \partial\Omega, \end{aligned}$$

with $\alpha = 1$, $\boldsymbol{\beta} = \langle 0, -1 \rangle$, and $f = 0$. Its exact solution is

$$u(x,y) = \frac{x(1 - e^{(y-1)/\alpha})}{1 - e^{-2/\alpha}},$$

and the boundary condition g is given from the exact.

In Figure 6.2, the rates of convergence in the A-norm error and the discrete L^∞-norm error are shown. The convergence rates in the A-norm error for the mesh types are consistent with the theoretical convergence error estimate in Theorem 5.2. Some superconvergence is shown with the mesh types `para` and `ncvx`. This is because the mesh types basically consist of structured polygons and the mesh-dependent norms are computed on them. It is easy to see that the EAVE method provides good approximations at the internal vertices of the mesh types by checking the discrete L^∞-norm errors. We note that the bilinear form $S_{\mathcal{E}}^K(\cdot,\cdot)$ in (3.13) was applied to get the results in Figure 6.2, and the other one $S_{\mathcal{V}}^K(\cdot,\cdot)$ in (3.12) gave similar results.

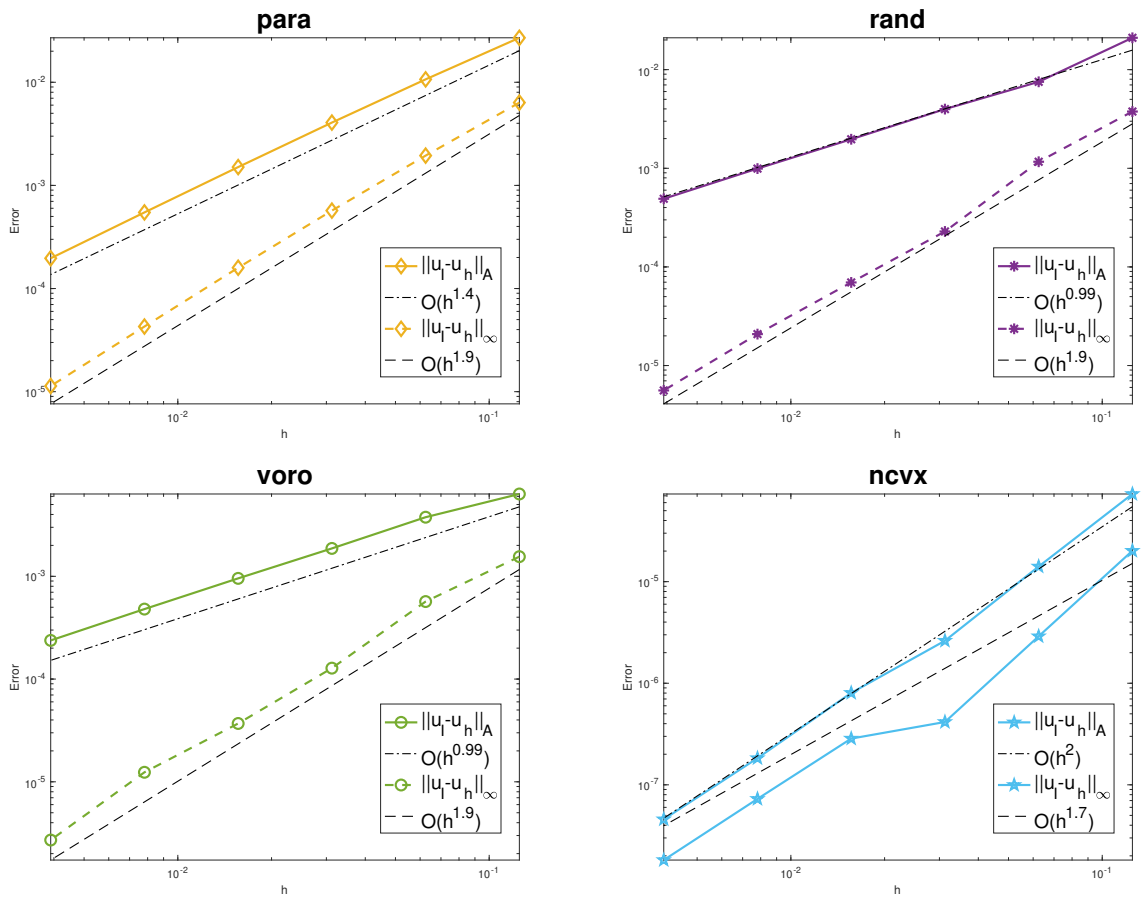

Figure 6.2: Convergence rate of the mesh-dependent norm errors (*test problem 1*).

6.2 Convection-Dominated Problems

The main goal of using the EAVE method is to get stable discrete solutions to convection-diffusion problems in the convection-dominated regime. The stable solution means a discrete solution without spurious oscillations or with smaller oscillations as well as it captures sharp boundary layers. Since the size of sharp layers usually depends on the diffusion coefficient, the coefficient is chosen in the intermediate regime or little bit smaller (compared to the range of the mesh size h that we use). Moreover, one can see that the seminorm $|J(u)|_{W^{1,s}(K)}$ belongs to the error bound in Theorem 5.2. Hence, extremely sharp layers would deteriorate the rate of convergence.

Test problem 2: Convection-dominated with a sharp layer

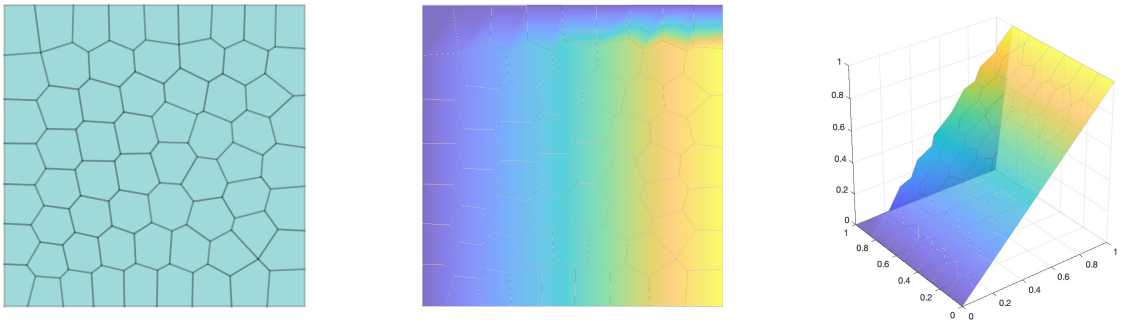

Figure 6.3: The interpolant of the exact solution, u_I, on the mesh `voro` (*test problem 2*).

We consider the convection-dominated problem presented in [36],

$$\begin{cases} -\nabla \cdot (\epsilon \nabla u + \boldsymbol{\beta} u) = f & \text{in } \Omega = (0,1) \times (0,1), \\ u = g & \text{on } \partial\Omega, \end{cases}$$

with $\epsilon = 10^{-2}$, $\boldsymbol{\beta} = \langle 0, -1 \rangle$, and $f = 0$. The exact solution is given as

$$u(x,y) = x \left(\frac{1 - e^{(y-1)/\epsilon}}{1 - e^{-2/\epsilon}} \right),$$

and the boundary condition comes from the exact solution (see Figure 6.3). We can see that the exact solution has sharper boundary layer around $y = 1$ when ϵ becomes smaller.

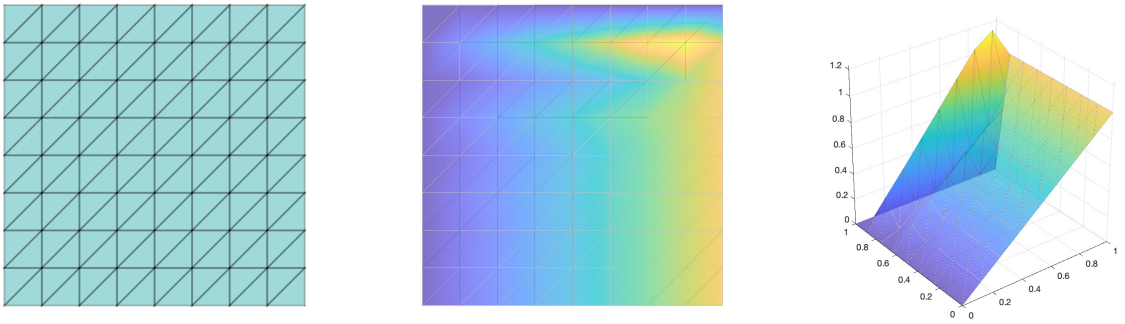

Figure 6.4: The SUPG solution when $\epsilon = 1/64$ and $h = 1/8$ (*test problem 2*).

In [36], the SUPG method [27] was applied to solve this problem. The numerical results in [36] showed the H^1-seminorm error of the SUPG solution is smaller than that of the standard FEM solution. However, even though the local error except the boundary layer was very small, the global error slowly decreased as the grid is successively refined. Figure 6.4 also shows that the SUPG solution is highly oscillatory around the boundary layer, and the spurious oscillations seem to propagate into the domain.

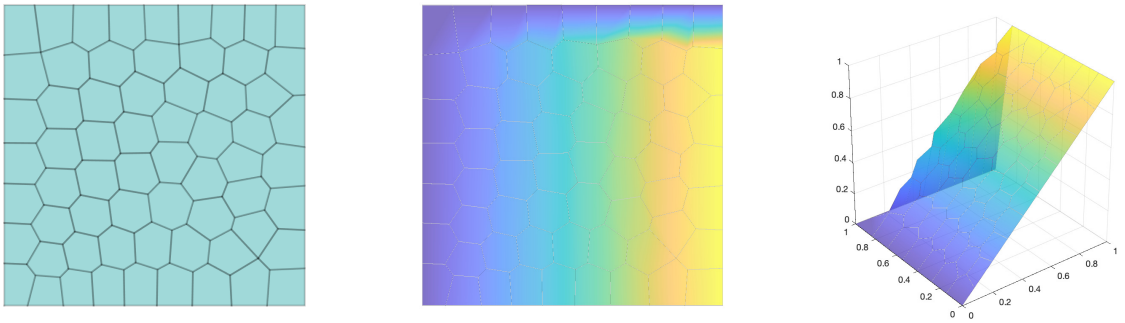

Figure 6.5: The EAVE solution with the bilinear form $S_{\mathcal{V}}^K$ on `voro` (*test problem 2*).

On the other hand, we apply the EAVE method with the stiffness matrix for the Poisson equation with the virtual bilinear form,

$$a_h^K(u_h, v_h) = \int_K \nabla \Pi_1^\nabla u_h \cdot \nabla \Pi_1^\nabla v_h \, d\mathbf{x} + S_{\mathcal{V}}^K(u_h - \Pi_1^\nabla u_h, v_h - \Pi_1^\nabla v_h).$$

One can find the exact definition of $S_{\mathcal{V}}^K$ in (3.12). As we see in Figure 6.5, the EAVE solution has no such oscillation, and seems to properly capture the boundary layer on the mesh `voro`.

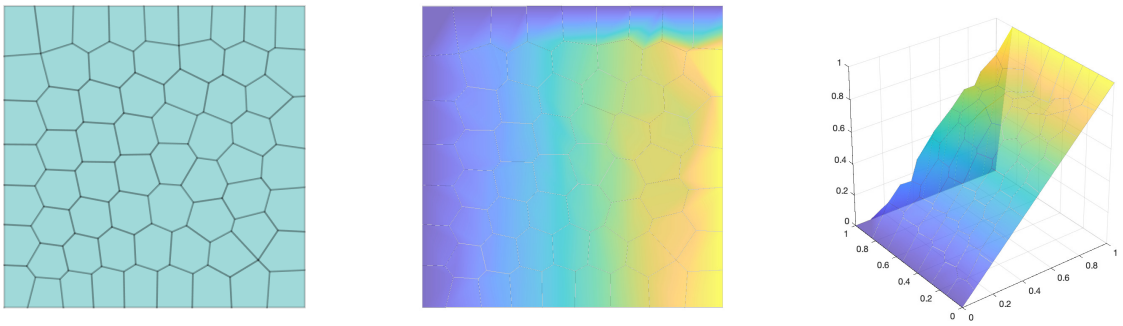

Figure 6.6: The EAVE solution with the bilinear form $S_{\mathcal{E}}^K$ on `voro` (*test problem 2*).

We also tested the other bilinear form $S_{\mathcal{E}}^K$ presented in (3.13). The EAVE solution with $S_{\mathcal{E}}^K$ is shown in Figure 6.6. Even though there is no severe oscillation around the boundary layer, the solution contains minor oscillations around the yellow part. We expect that this

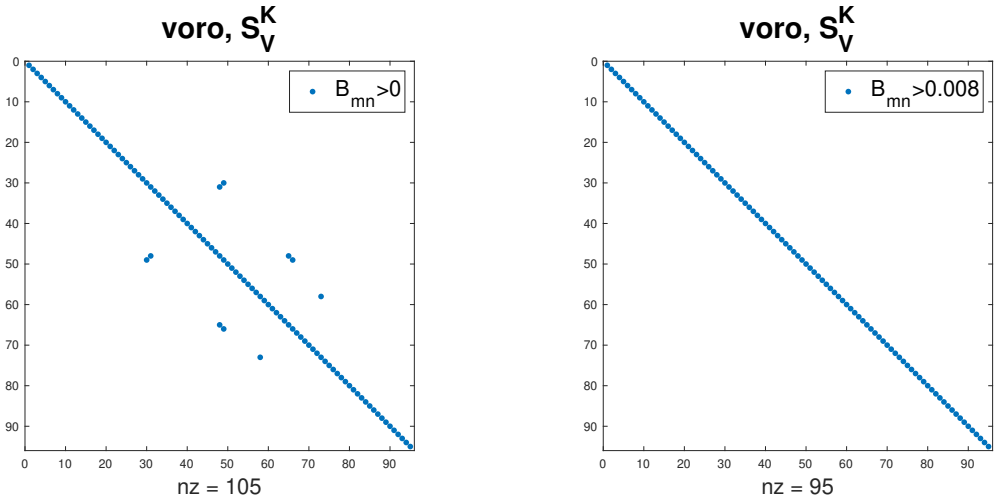

Figure 6.7: The information of positive components in the stiffness matrices with $S_{\mathcal{V}}^K$.

phenomenon is related to the M-matrix condition or monotonicity of the the stiffness matrix of the EAVE method,

$$B_{mn} = \sum_{K \in \mathcal{K}_h} B_h^K(\phi_n, \phi_m).$$

Figure 6.7 shows the information of positive components in the stiffness matrix with $S_{\mathcal{V}}^K$. We find some positive off-diagonal entries, so the stiffness matrix on the mesh `voro` fails the M-matrix condition. However, the maximum value among the positive off-diagonal entries is 0.0074 (see the right plot in Figure 6.7) while the minimum of the diagonal entries is 0.0695. This implies that the stiffness matrix is diagonally dominant, and it contains only small positive off-diagonal entries. These two conditions lead the stiffness matrix to partially satisfy the Lorenz's sufficient condition for monotonicity [44] (see also [43]). The Lorenz's condition is known as a sufficient condition for monotonicity when the stiffness matrix is not an M-matrix, and this condition implies that the stiffness matrix is the product of two nonsingular M-matrices. Therefore, even though the stiffness matrix is not an M-matrix, it would be possible to see that the matrix implies monotonicity.

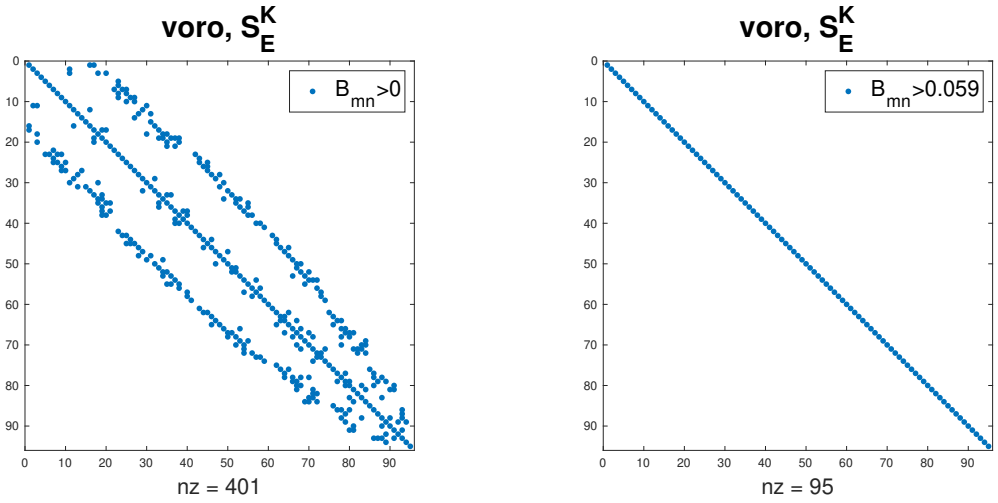

Figure 6.8: The information of positive components in the stiffness matrices with $S_{\mathcal{E}}^K$.

In Figure 6.8, we can see that the stiffness matrix with $S_{\mathcal{E}}^K$ has more positive off-diagonal entries than $S_{\mathcal{V}}^K$. The maximum of the positive off-diagonal entries is 0.0590, and the minimum of diagonal entires is 0.1195. Hence, compared to the stiffness matrix with $S_{\mathcal{V}}^K$, it is not likely that the stiffness matrix with $S_{\mathcal{E}}^K$ is monotone.

Furthermore, convergence rates of the mesh-dependent norm errors with $S_{\mathcal{V}}^K$ are presented in Figure 6.9 and 6.10. The convergence rate (`para`) means that the EAVE solution on the

parallelograms is the same as the interpolant u_I of the exact solution at the structured grid points. The mesh type `ncvx` has super-convergence because this mesh has structured grid

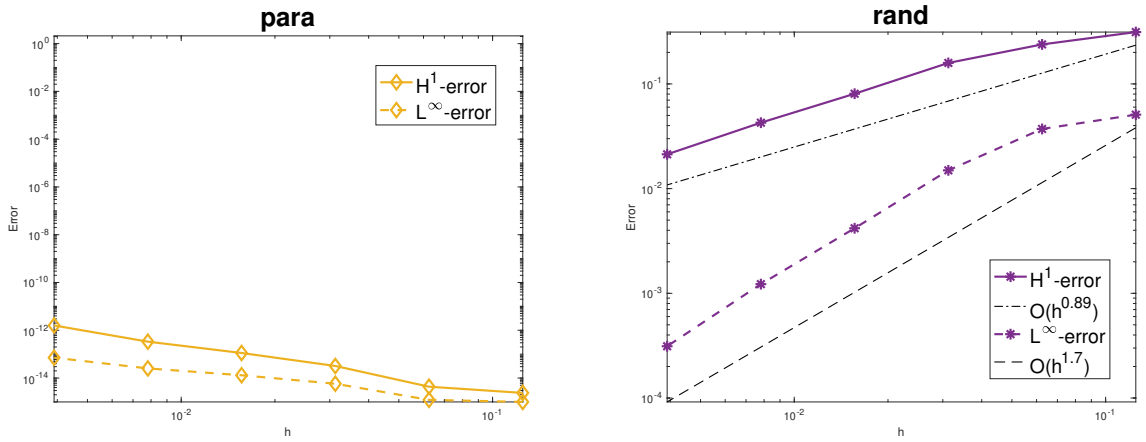

Figure 6.9: Convergence rate of the mesh-dependent norm errors with $S_{\mathcal{V}}^K$ (*test problem 2*).

points. When the random polygonal mesh (`rand`) and optimized polygonal mesh (`voro`) are given, the mesh dependent A-norm error has the first order convergence rate. The mesh dependent L^∞-norm error almost has the second order convergence rate, and it implies that there is no severe oscillation observed in the SUPG solution.

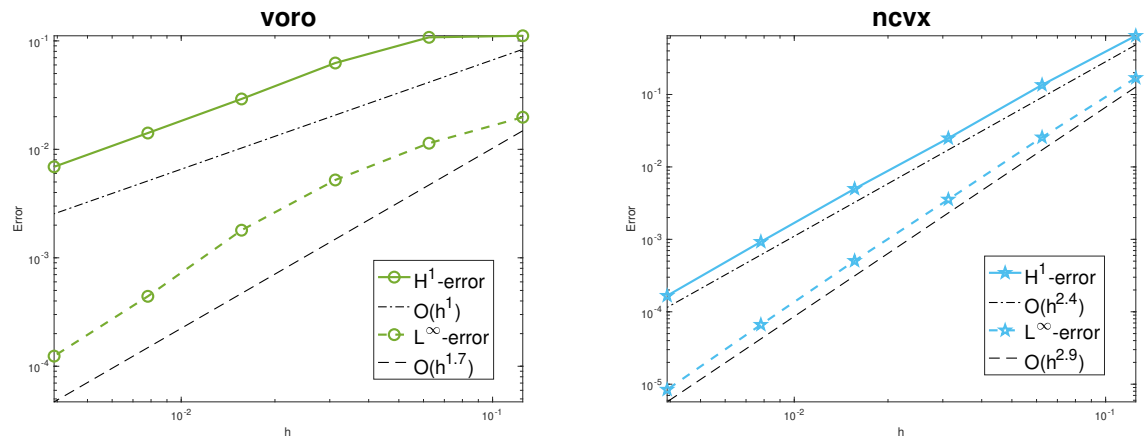

Figure 6.10: Convergence rate of the mesh-dependent norm errors with $S_{\mathcal{V}}^K$ (*test problem 2*).

With the bilinear form $S_{\mathcal{E}}^K$, we check the convergence rates of the mesh-dependent norm errors. Figure 6.11 and 6.12 show the convergence rates in the different mesh types. On the structured meshes `para` and `ncvx`, it is shown that the A-norm errors have super-convergence.

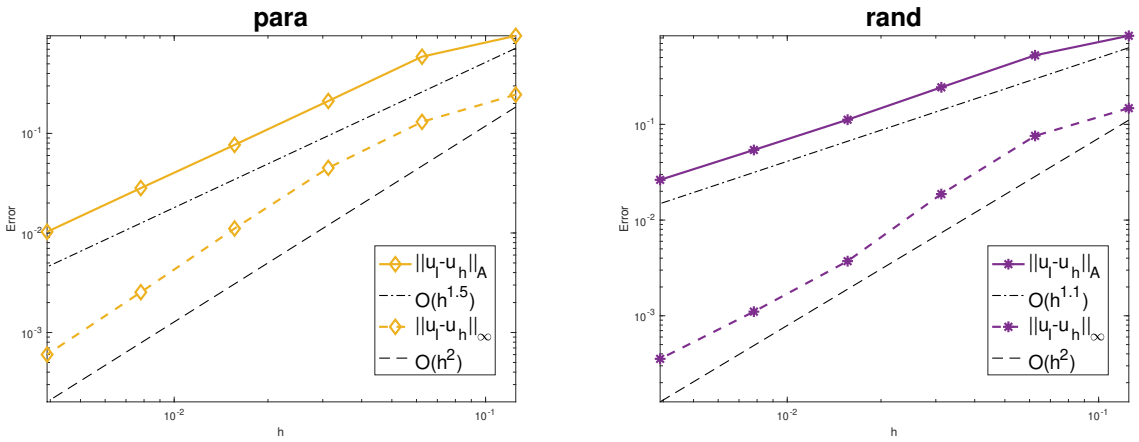

Figure 6.11: Convergence rate of the mesh-dependent norm errors with $S_{\mathcal{E}}^K$ (*test problem 2*).

Compared to the convergence rate with $S_{\mathcal{V}}^K$, even though the numerical solution has small oscillations, the convergence rates of the A-norm errors look faster in the mesh type `rand` and `voro`. The L^∞-norm errors also tend to decrease faster. This implies that the small

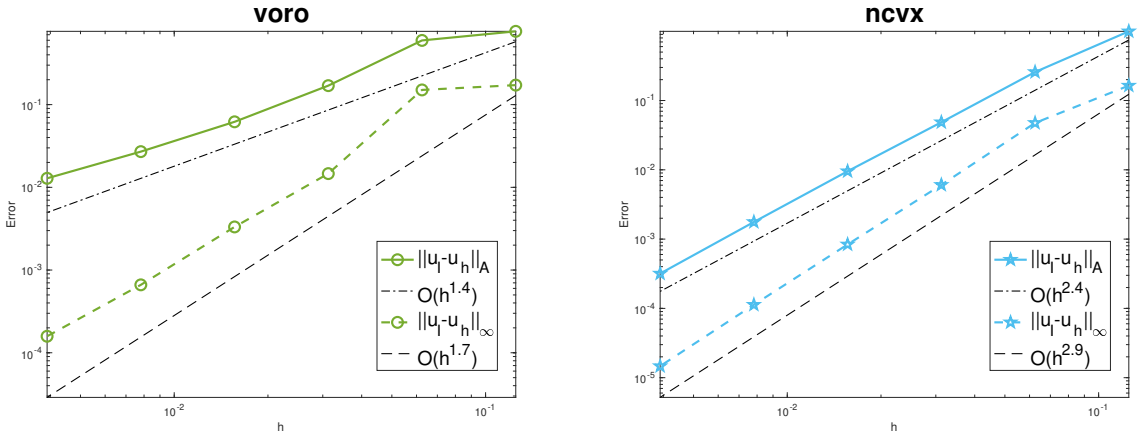

Figure 6.12: Convergence rate of the mesh-dependent norm errors (*test problem 2*).

oscillations are suppressed as the meshes are refined, and the shape boundary layer is resolved when small mesh size is applied.

For example, Figure 6.13 displays the EAVE solution with $S_{\mathcal{E}}^K$ and the mesh type `voro` when $\epsilon = 10^{-2}$ and $h = 1/32$, and Figure 6.14 shows the EAVE solution with the mesh type `rand`. We saw from Figure 6.6 that the EAVE solution with $S_{\mathcal{E}}^K$ had small oscillations when $h = 1/8$, but we can see from Figure 6.13 that such oscillations disappear and the boundary

layer is perfectly resolved when $h = 1/32$. Similarly, on the random polygonal mesh `rand`,

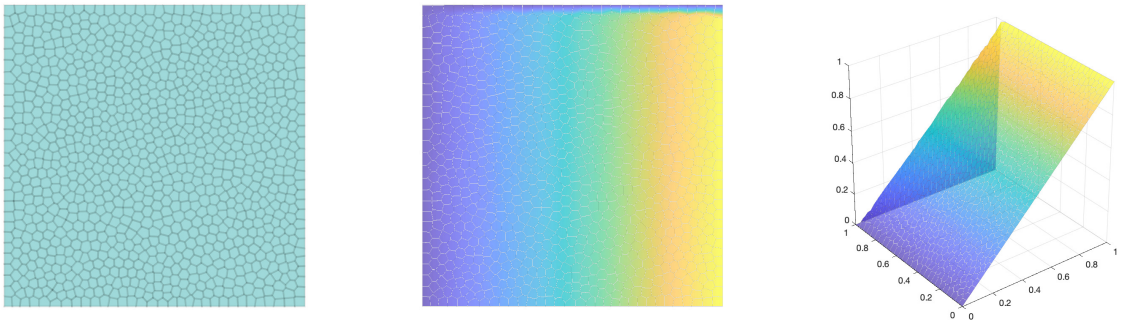

Figure 6.13: The EAVE solution with the bilinear form $S_{\mathcal{E}}^{K}$ on refined `voro` (*test problem 2*).

we obtain a quality discrete solution capturing the sharp boundary layer without spurious oscillations when $h = 1/32$.

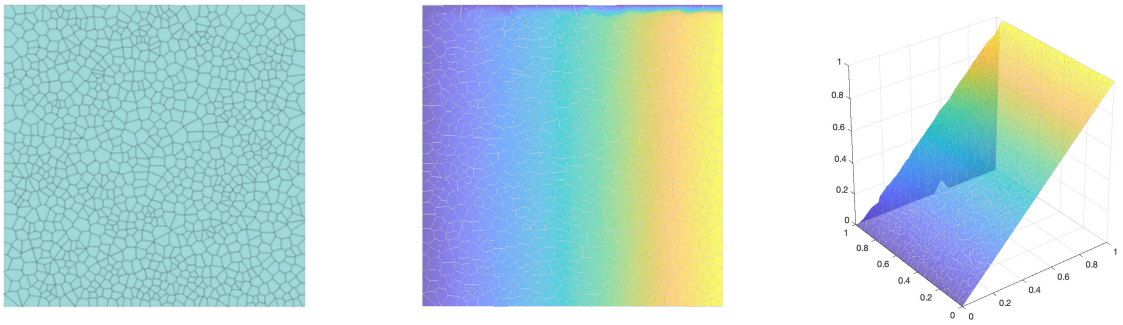

Figure 6.14: The EAVE solution with the bilinear form $S_{\mathcal{E}}^{K}$ on refined `rand` (*test problem 2*).

Through this test problem, we can see that the EAVE method provides discrete solutions without spurious oscillations or with smaller oscillations while resolving the sharp boundary layer. It is shown that random polygonal meshes can be applied as well as the EAVE solutions are better than the SUPG solutions in this test problem. See also the following figures.

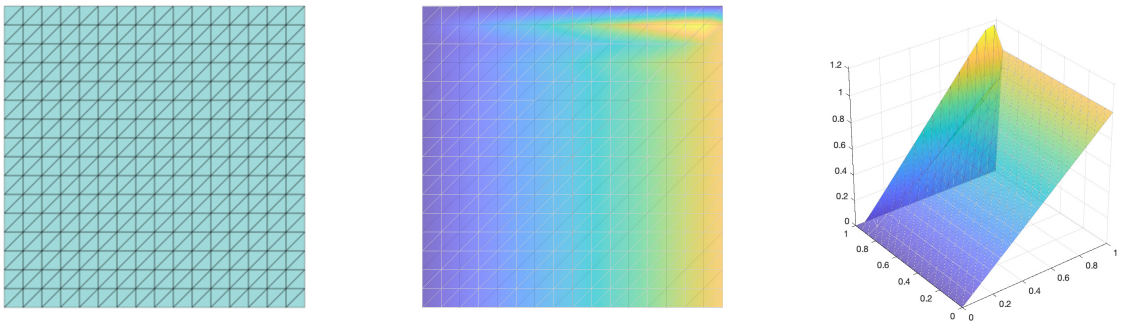

Figure 6.15: The SUPG solution when $\epsilon = 10^{-2}$ and $h = 1/16$ (*test problem 2*).

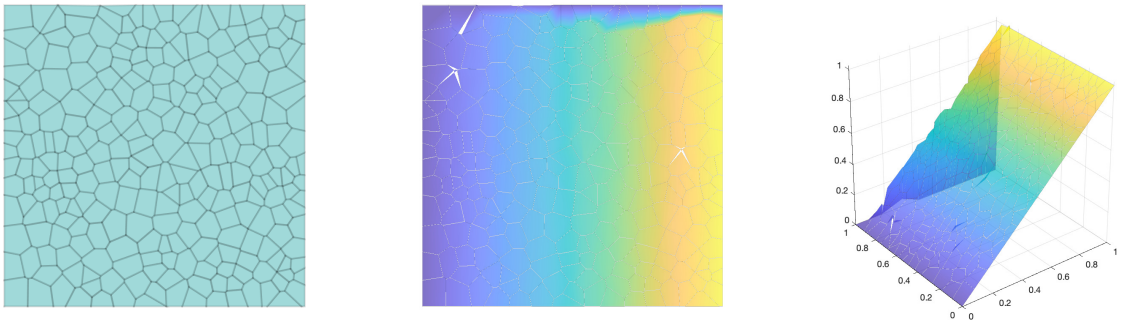

Figure 6.16: The EAVE solution with the bilinear form $S_{\mathcal{V}}^{K}$ on refined `rand` (*test problem 2*).

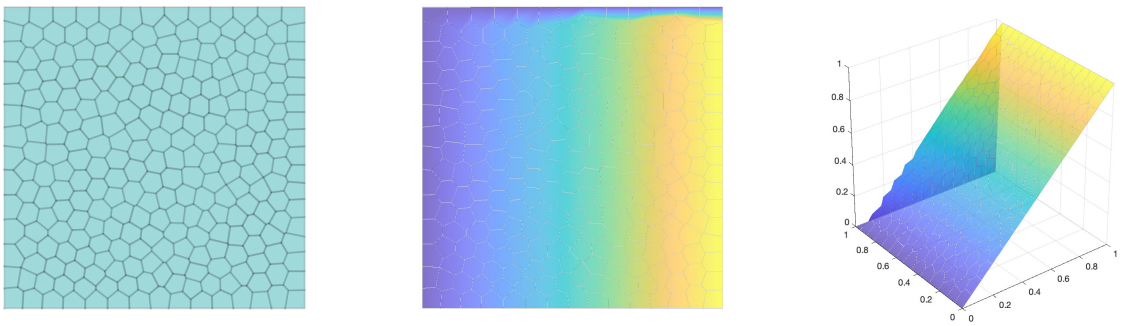

Figure 6.17: The EAVE solution with the bilinear form $S_{\mathcal{V}}^{K}$ on refined `voro` (*test problem 2*).

Test Problem 3: Extremely sharp boundary layers

We consider the same convection-diffusion equation $-\nabla \cdot (\epsilon \nabla u + \boldsymbol{\beta} u) = f$ with

$$\epsilon = 10^{-9}.$$

The other conditions are the same as the test problem 2. Since the seminorm $|J(u)|_{W^{1,s}(K)}$

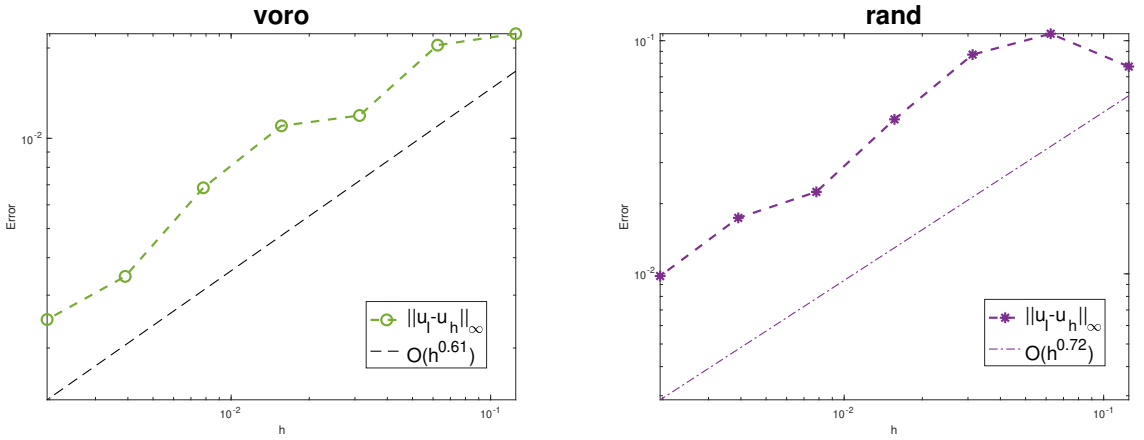

Figure 6.18: Convergence rate of the mesh-dependent norm errors (*test problem 3*).

is contained in the H^1-norm error bound in Theorem 5.2, it is not possible to obtain a reasonable rate of convergence in the mesh-dependent A-norm. More exactly, ∇u around the boundary layer depends on ϵ^{-1}, so adaptive mesh refinement is needed to capture the layer.

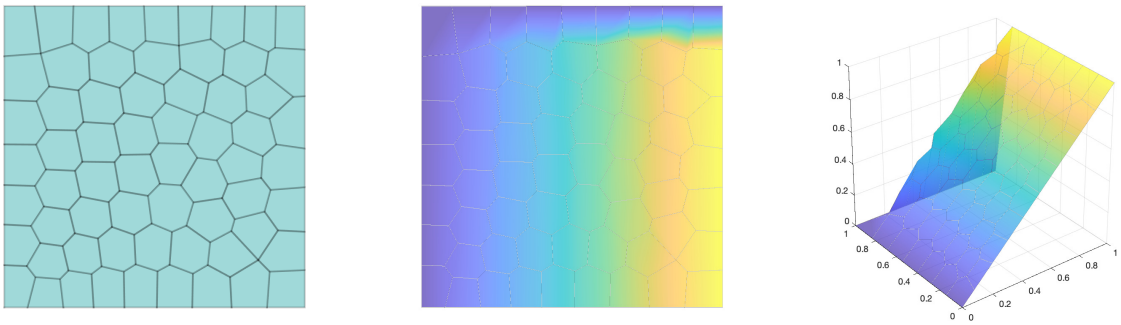

Figure 6.19: The EAVE solution with the bilinear form $S_{\mathcal{V}}^K$ on `voro` (*test Problem 3*).

However, we can obtain stable solutions to the test problem by using the EAVE method, and the convergence is verified by the mesh-dependent L^∞-norm error (see Figure 6.18).

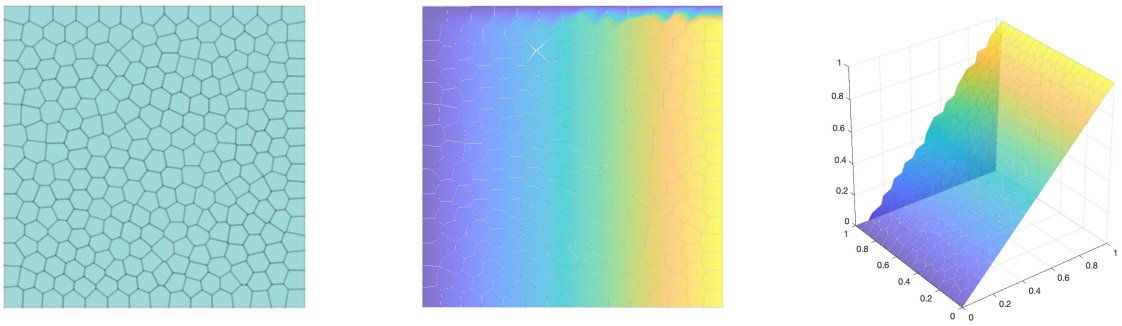

Figure 6.20: The EAVE solution with the bilinear form $S_{\mathcal{V}}^K$ on refined `voro` (*test Problem 3*).

In Figure 6.19, we are convinced that the EAVE solution on the `voro` mesh is stable while the solution resolves the sharp boundary layer within the give mesh size. Figure 6.20 shows that the EAVE solution on the refined mesh contains a shaper boundary layer.

Bibliography

[1] R. A. Adams and J. F. Fournier, *Sobolev Spaces*, Academic Press, New York, 1978.

[2] D. Adak and E. Natarajan, A unified analysis nonconforming virtual element methods for convection diffusion reaction problem, arXiv:1601.01077.

[3] B. Ahmad, A. Alsaedi, F. Brezzi, L. Marini, and A. Russo, Equivalent projectors for virtual element methods, *Comput. Math. Appl.*, 66(3): 376–391, 2013.

[4] P. Antonietti, G. Manzini, and M. Verani, The fully nonconforming virtual element method for biharmonic problems, *Mathematical Models and Methods in Applied Sciences*, 28, 2016.

[5] M. Arroyo and M. Ortiz Local *maximum-entropy* approximation schemes: a seamless bridge between finite elements and meshfree methods *Int. J. Numer. Meth. Engng*, 65, 2167–2202, 2006.

[6] G. Auchmuty and J. C. Alexander, L^2 well-posedness of planar Div-Curl system, *Arch. Rational Mech. Anal.*, 160: 91–134, 2001.

[7] B. Ayuso de Dios, K. Lipnikov, and G. Manzini, The nonconforming virtual element method, arXiv:1405.3741, 2014.

[8] I. Babuška, U. Banerjee, and J. E. Osborn, Survey of meshless and generalized finite element methods: A unified approach, *Acta Numerica*, 12: 1–125, 2003.

[9] C. Bacuta, J. H. Bramble, and J. Xu, Regularity estimates for elliptic boundary value problems in Besov spaces, *Mathematics of Computation*, 72(244): 1577-1595, 2002.

[10] R. E. Bank, P. S. Vassilevski, and L. T. Zikatanov, Arbitrary dimension convection-diffusion schemes for space-time discretizations, *Journal of Computational and Applied Mathematics*, 310: 19–31, 2017.

[11] Gabriel R. Barrenechea, Volker John, Petr Knobloch, and Richard Rankin, A unified analysis of algebraic flux correction schemes for convection-diffusion equations, *SeMA* 75: 655–685, 2018.

[12] L. Beirão da Veiga, F. Brezzi, A. Cangiani, G. Manzini, L. D. Marini, and A. Russo, Basic principles of virtual element methods, *Math. Models Methods Appl. Sci.* 23(1): 199–214, 2013.

[13] L. Beirão da Veiga, F. Brezzi, L. D. Marini, and A. Russo, The Hitchhiker's guide to the virtual element method, *Math. Models Methods Appl. Sci.* 24(8): 1541–1573, 2014.

[14] L. Beirão da Veiga, F. Brezzi, L. D. Marini, and A. Russo, Mixed Virtual Element Methods for general second order elliptic problems on polygonal meshes, arXiv:1506.07328, 2015.

[15] L. Beirão da Veiga, F. Brezzi, L. Marini, and A. Russo, Serendipity nodal VEM spaces, *Computers and Fluids*, 141: 2–12, 2016.

[16] L. Beirão da Veiga, F. Brezzi, L. Marini, and A. Russo, Virtual element methods for general second order elliptic problems on polygonal meshes, *Math. Models Methods Appl. Sci.*, 26(4): 729–750, 2016.

[17] L. Beirão da Veiga, F. Brezzi, L. D. Marini, and A. Russo, $H(\mathrm{div})$ and $H(\mathrm{curl})$-conforming VEM, *Numer. Math.*, 133(2): 303–332, 2016.

[18] L. Beirão da Veiga, F. Brezzi, F. Dassi, L. D. Marini, and A. Russo, Virtual element approximation of 2D magnetostatic problems, *Comput. Methods Appl. Mech. Engrg.*, 327: 173–195, 2017.

[19] L. Beirão da Veiga, F. Brezzi, L. D. Marini, and A. Russo, Serendipity face and edge VEM spaces, *Rend. Lincei Mat. Appl.* 28(1): 143–180, 2017.

[20] L. Beirão da Veiga, F. Brezzi, F. Dassi, L. Marini, and A. Russo, Lowest order virtual element approximation of magnetostatic problems, *Comput. Methods Appl. Mech. Engrg.*, 332: 343–362, 2018.

[21] L. Beirão da Veiga, F. Dassi, C. Lovadina, and G. Vacca, SUPG-stabilized virtual elements for diffusion-convection problems: a robustness analysis, arXiv:2012.01104, 2020.

[22] L. Beirão da Veiga, F. Dassi, and A. Russo A C^1 virtual element method on polyhedral meshes, *Computers & Mathematics with Applications*, 79(7), 1936–1955, 2020.

[23] M. F. Benedetto, S. Berrone, A. Borio, S. Pieraccini, and S. Scialò, Order preserving SUPG stabilization for the virtual element formulation of advection-diffusion problems, *Comput. Methods Appl. Mech. Engrg.*, 311: 18–40, 2016.

[24] S. Berrone, A. Borio, and G. Manzini, SUPG stabilization for the nonconforming virtual element method for advection-diffusion-reaction equations, *Comput. Methods Appl. Mech. Engrg.*, 340: 500–529, 2018.

[25] S. C. Brenner, L. R. Scott, *The Mathematical Theory of Finite Element Methods*, Springer, New York, 2008.

[26] S. C. Brenner, Q. Guan, and L. Sung, Some estimates for virtual element methods, *Comput. Methods Appl. Math.*, 17(4): 553–574, 2017.

[27] A. N. Brooks and T. J.R. Hughes, Streamline upwind/Petrov-Galerkin formulations for convection dominated flows with particular emphasis on the incompressible Navier-Stokes equations, *Comput. Methods Appl. Mech. Eng.*, 32(1-3), 199–259, 1982.

[28] E. Burman and P. Hansbo, Edge stabilization for Galerkin approximations of convection-diffusion-reaction problems, *Comput. Methods Appl. Mech. Eng.*, 193(15-16), 1437–1453, 2004.

[29] A. Cangiani, E. H. Georgoulis, and P. Houston, hp-version discontinuous Galerkin methods on polygonal and polyhedral meshes, *Mathematical Models and Methods in Applied Sciences*, 24(10): 2009–2041, 2014.

[30] A. Cangiani, G. Manzini, and O. Sutton, Conforming and nonconforming virtual element methods for elliptic problems, *IMA Journal of Numerical Analysis*, 37: 1317–1354, 2017.

[31] S. Cao and L. Chen, Anisotropic error estimates of the linear virtual element method on polygonal meshes, *SIAM J. NUMER. ANAL.*, 56(5): 2913–2939, 2018.

[32] L. Chen, *iFEM: An Integrated Finite Element Methods Package in MATLAB*, Technical Report, University of California at Irvine, 2009.

[33] L. Chen and J. Huang, Some error analysis on virtual element methods, *Calcolo*, 55(1): 1–23, 2018.

[34] M. Dauge, *Elliptic Boundary Value Problems on Corner Domains*, Lecture notes in mathematics 1341, Springer-Verlag, Berlin, 1988.

[35] T. Dupont and L. R. Scott, Polynomial approximation of functions in Sobolev spaces, *Mathematics of Computation*, 34(150): 441–463, 1980.

[36] H. Elman, D. Silvester, and A. Wathen, *Finite Element and Fast Iterative Solvers*,

Numerical Mathematics and Scientific Computation, Oxford University Press, Oxford, 2005.

[37] D. Gilbarg and N. S. Trudinger, *Elliptic Partial Differential Equations of Second Order*, Classics in Mathematics, Springer-Verlag, Berlin, 1983.

[38] J. Jia, X. Hu, J. Xu, and C. S. Zhang, Effects of integrations and adaptivity for the Eulerian-Lagrangian method, *Journal of Computational Mathematics*, 29(4): 367–395, 2011.

[39] V. John, Petr Knobloch, and Julia Novo, Finite elements for scalar convection-dominated equations and incompressible flow problems: a never ending story? *Computing and Visualization in Science*, 19: 47–63, 2018.

[40] Interpolation between subspaces of a Hilbert space, Technical note BN-719, Institute for Fluid Dynamics and Applied Mathematics, University of Maryland, College Park, 1971.

[41] P. Knobloch, A generalization of the local projection stabilization for convection-diffusion-reaction equations, *SIAM J. Numer. Anal.* 48(2): 659–680, 2010.

[42] R. D. Lazarov and L. T. Zikatanov, An exponential fitting scheme for general convection-diffusion equations on tetrahedral meshes, *Comput. Appl. Math.*, 1(92): 60–69, 2005.

[43] H. Li and X. Zhang, On the monotonicity and discrete maximum principle of the finite difference implementation of C^0-Q^2 finite element method, *Numer. Math.* 145: 437–472, 2020.

[44] J. Lorenz, Zur inversemonotonie diskreter probleme, *Numer. Math.* 27(2): 227–238, 1977.

[45] E. D. Nezza, G. Palatucci, and E. Valdinoci, Hitchhiker's guide to the fractional Sobolev spaces, arXiv:1104.4345, 2011

[46] N. Sukumar and A. Tabarraei, Conforming polygonal finite elements, *Int. J. Numer. Meth. Engng*, 61: 2045-2066, 2004.

[47] M. Stynes, Steady-state convection-diffusion problems, *Acta Numerica*, 14: 445–508, 2005.

[48] C. Talischi, G. H. Paulino, A. Pereira, and I. F. M. Menezes, `PolyMesher`: a general-purpose mesh generator for polygonal elements written in Matlab. *Structural Multidisciplinary Optimization*, 45, 309–328, 2012.

[49] J. Xu and L. T. Zikatanov, A monotone finite element scheme for convection-diffusion equations, *Mathematics of Computation*, 68(228): 1429–1446, 1999.

Appendix A

Proof of the Norm Equivalence

Main statement in of lemma 5.1

Let $\mathbb{V}_h(K)$ be a finite dimensional subspace of $L^p(K)$ for any $p > 1$. Then, every element $\mu \in \mathbb{V}_h(K)$ satisfies

$$\|\mu\|_{L^p(K)} \leq C h_K^{2/p-1} \|\mu\|_{L^2(K)},$$

where C is a generic constant independent of h_K.

Proof

If $p < 2$, it is straightforward to show the inequality (5.1) using Hölder's inequality. For any $p > 2$, we use the argument presented in [33] so that it suffices to prove the estimate (5.1) with scaled elements $\hat{K} := \{\hat{\mathbf{x}} \mid \hat{\mathbf{x}} = \mathbf{x}/h_K, \mathbf{x} \in K\}$ and scaled functions $\hat{\mu}(\hat{\mathbf{x}}) := \mu(h_K\hat{\mathbf{x}}) = \mu(\mathbf{x})$. Let $\hat{\mathcal{K}}$ be the set of all scaled polygons satisfying the shape regularity assumptions [26, 33]. Since all norms on finite-dimensional vector spaces are equivalent (see details in [25]), we

define

$$C(\hat{K}) := \sup_{\hat{\mu} \in \mathbb{V}_h(\hat{K})} \frac{\|\hat{\mu}\|_{L^p(\hat{K})}}{\|\hat{\mu}\|_{L^2(\hat{K})}} \tag{A.1}$$

for any polygon $\hat{K} \in \hat{\mathcal{K}}$. We prove that $C(\hat{K})$ is continuous with respect to $\hat{K}$ in a compact set $\hat{\mathcal{K}}$, which implies that $C(\hat{K})$ is uniformly bounded for $\hat{K} \in \hat{\mathcal{K}}$.

Let $\hat{K}^\varepsilon := \tau_\varepsilon(\hat{K})$ be a small perturbation of $\hat{K}$ using a mapping τ_ε. The mapping τ_ε is explicitly defined as follows: For a finite number of points on $\partial\hat{K}$ including all the vertices, a triangulation of $\hat{K}$ is defined with a point inside $\hat{K}$ because $\hat{K}$ is a star-shaped polygon. While the points on $\partial\hat{K}$ slightly move a distance of ε, affine mappings from triangles in $\hat{K}$ to those in $\hat{K}^\varepsilon$ are defined (e.g. Figure 6.1), and each of the affine mappings converges to the identity map as ε goes to 0.

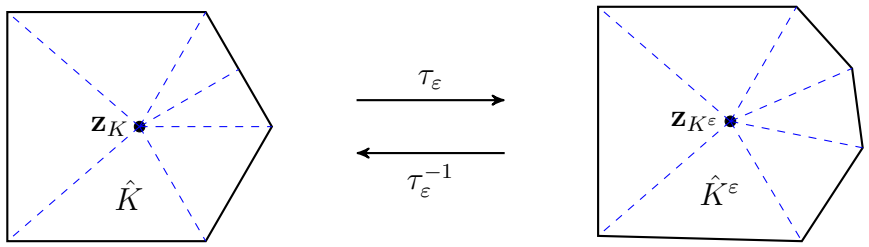

Figure A.1: An example of the mapping τ_ε from $\hat{K}$ to $\hat{K}^\varepsilon$

Let $\mu_* \in \mathbb{V}_h(\hat{K})$ be the maximizer of (A.1), that is, $C(\hat{K}) = \|\mu_*\|_{L^p(\hat{K})}/\|\mu_*\|_{L^2(\hat{K})}$. For every $\varepsilon > 0$, we define $\mu_*^\varepsilon := \mu_* \circ \tau_\varepsilon^{-1} \in \mathbb{V}_h(\hat{K}^\varepsilon)$ which converges pointwise to μ_* as ε approaches to 0. Then, it is straightforward to verify that $\|\mu_*^\varepsilon\|_{L^p(\hat{K}^\varepsilon)}$ and $\|\mu_*^\varepsilon\|_{L^2(\hat{K}^\varepsilon)}$ are converging to $\|\mu_*\|_{L^p(\hat{K})}$ and $\|\mu_*\|_{L^2(\hat{K})}$, respectively. Hence, we have

$$C(\hat{K}^\varepsilon) \geq \frac{\|\mu_*^\varepsilon\|_{L^p(\hat{K}^\varepsilon)}}{\|\mu_*^\varepsilon\|_{L^2(\hat{K}^\varepsilon)}} \;\to\; \frac{\|\mu_*\|_{L^p(\hat{K})}}{\|\mu_*\|_{L^2(\hat{K})}} = C(\hat{K}) \quad \text{as} \quad \varepsilon \to 0.$$

On the other hand, let $\mu_\dagger^\varepsilon \in \mathbb{V}_h(\hat{K}^\varepsilon)$ be the maximizer for $C(\hat{K}^\varepsilon)$ for every $\varepsilon > 0$, and $\mu_\dagger := \mu_\dagger^\varepsilon \circ \tau_\varepsilon$. Then, it follows that $C(\hat{K}^\varepsilon) \leq C(\hat{K})$ as ε goes to 0.